American Mineralogist, Volume 96, pages 1686–1702, 2011

The crystal structure of franckeite, $Pb_{21.7}Sn_{9.3}Fe_{4.0}Sb_{8.1}S_{56.9}$

E. Makovicky,[1,*] V. Petříček,[2] M. Dušek,[2] and D. Topa[3]

[1]Department of Geography and Geology, University of Copenhagen, Østervoldgade 10, DK1350 Copenhagen, Denmark
[2]Institute of Physics, Czech Academy of Sciences, Na Slovance 2, CZ-18040 Prague 8, Czech Republic
[3]Department of Material Research and Physics, University of Salzburg, Hellbrunnerstrasse 34, A-5020 Salzburg, Austria

Abstract

The layer-like crystal structure of franckeite from the mine of San José, Bolivia, exhibits a pronounced one-dimensional transversal wave-like modulation and a non-commensurate layer match in two dimensions. It consists of alternating pseudohexagonal (H) layers and pseudotetragonal (Q) slabs and forms a homologous pair with cylindrite, which has thinner Q slabs. The Q slabs in franckeite are four atomic layers thick. The two components have their own lattices and a common modulation. The Q slab of the refined franckeite structure, $Pb_{21.74}Sn_{9.34}Fe_{3.95}Sb_{8.08}S_{56.87}$, is an MS layer (M = Pb^{2+}, Sn^{2+}, Sb^{3+}) four atomic planes thick, with a = 5.805(8), b = 5.856(16) Å, and the layer-stacking vector c = 17.338(5) Å. The lattice angles are α = 94.97(2)°, β = 88.45(2)°, γ = 89.94(2)°; the modulation vector q = –0.00129(8) **a*** + 0.128436(10) **b*** – 0.0299(3) **c***. The H layer is a single-octahedron MS_2 layer (M = Sn^{4+}, Fe^{2+}) with a = 3.665(8), b = 6.2575(16), c = 17.419(5) Å, α = 95.25(2)°, β = 95.45(2)°, γ = 89.97(2)°; the modulation vector is q = –0.00087(8) **a*** + 0.13725(16) **b*** – 0.0314(4) **c***. The **a** and **b** vectors of both subsystems are parallel; the **c** vectors diverge. (3+2)D superspace refinement was performed in the superspace group $C\bar{1}$, using 7397 observed reflections. It resulted in the overall R(obs) value equal to 0.094. The Q slabs are composed of two tightly bonded double-layers, separated by an interspace hosting non-bonding electron pairs. Average composition of cations on the outer surface was refined as $Pb_{0.74}(Sn,Sb)_{0.26}$, whereas that of cations, which are adjacent to the interspace with lone electron pairs, with a configuration analogous to that observed in orthorhombic SnS, corresponds to $(Sn,Sb)_{0.73}Pb_{0.27}$. Iron is dispersed over the octahedral Sn^{4+} sites in the H layer. Transversal modulation of the Q slab is achieved by local variations in the Pb:(Sn,Sb) ratios at its surface and interior. Its purpose is to re-establish a one-dimensional commensurate contact along [010] between the curved Q and H surfaces to the greatest extent possible. Layer-stacking disorder and divergence of the Q and H stacking directions, and the divergence between modulation wave-front and these stacking directions are typical for the composite structures of franckeite and cylindrite. Because of the increased rigidity of the Q component, franckeite usually forms masses of curved crystals rather than cylindrical aggregates. The existence of this family depends critically on the radius ratios of the cations involved, especially those involving (Pb^{2+}, Sn^{2+}) and Sn^{4+}. Their replacement by a Pb^{2+}:Bi^{3+} combination leads to misfit layer structures of a very different type, typified by cannizzarite.

Keywords: Franckeite, Pb-Sn-Sb-Fe sulfide, modulated layer-misfit crystal structure, 2D–non-commensurate layer structure, San José, Bolivia

Introduction and history of investigation

Franckeite is a complex sulfide of Pb, Sn^{2+}, Sn^{4+}, Sb, and Fe, described first by Stelzner (1893) from Bolivia. Until the 1970s it aroused little attention, mostly of field mineralogists (Bonshtedt-Kupletskaya and Chukhrov 1960), but after the interesting results of studies on related cylindrite (Makovicky 1970, 1974; Mozgova et al. 1975) became known, attention was directed to franckeite as well. X-ray crystallography of Sn-rich franckeite was described by Makovicky (1976), whereas that of Pb-rich franckeite by Wolf et al. (1981). They were described under the names incaite and potosiite, respectively. Li (1990) quotes additional crystallographic studies by Wang (1989); these data are summarized by Makovicky and Hyde (1992). Organova et al. (1980) published a Patterson function of franckeite but the work apparently did not proceed any further. Extensive HRTEM and electron diffraction study of franckeite was performed by Williams and Hyde (1988) and Williams (1989). Models of the crystal structure of franckeite in a projection along the non-modulated direction of a layer were constructed using the HRTEM data by these authors and by Wang (1989) and Wang and Kuo (1991). A STM study of a cleavage surface of franckeite was performed by Ma et al. (1997), whereas Henriksen et al. (2002) made a detailed study by STM and AFM. The classical chemical analyses of franckeite were summarized by Bonshtedt-Kupletskaya and Chukhrov (1960). Further contributions to the chemistry of franckeite were made by Makovicky (1974), Wolf et al. (1981), Williams (1989), and especially by Mozgova et al. (1975) and Bernhardt (1984), using electron microprobe. Synthetic studies performed by Li (1984) confirmed the idea, derived from chemical analyses, that

* E-mail: emilm@geo.ku.dk

franckeite is a broad solid-solution series with an extensive Pb for Sn^{2+} substitution.

Franckeite is a natural layer-misfit structure with two-dimensional non-commensurability of component layers, the second such structure after cylindrite. The purpose of the current study is to determine and refine the crystal structure of franckeite from X-ray diffraction data by means of superspace refinement as a clue to its remarkable properties and highly variable crystal chemistry.

Previous crystallographic studies

In the first single-crystal diffraction experiment on franckeite, Coulon et al. (1961) found only one component [the pseudotetragonal component of Makovicky (1974)], and they determined the monoclinic unit-cell parameters $a = 5.82(4)$, $b = 8 \times 5.86(1)$, $c = 17.3(5)$ Å, and $\beta = 94.66(25)°$ (in the orientation used in this paper). Makovicky (1974) stated that "incaite", a Sn-rich variety of franckeite, shows similar diffraction and compositional features (Table 1) as cylindrite, i.e., two component lattices described as a pseudotetragonal (T, later altered to Q) and a pseudohexagonal (H) component lattice. It has a longer layer-stacking c vector (our orientation) than cylindrite (17.29 Å for the Q component compared to 11.73 Å of cylindrite), which indicates thicker Q slabs. Makovicky's remark that the majority of franckeites show d_{001} spacing (our orientation) of ~17.3 Å, based especially on the powder diffraction data of Mozgova et al. (1975), was not pursued further. Trying to reconcile the crystallographic and electron microprobe data Makovicky (1976) and Makovicky and Hyde (1981) suggested that the Q slabs in incaite might have layer thickness 1.5 times that of cylindrite. Organova et al. (1980) performed a partial crystal structure determination on franckeite from Huanuni, Bolivia. Based on the published Patterson synthesis, they suggested that franckeite (layer stacking period equal to 17.4–17.7 Å) has four atomic layers thick pseudotetragonal slabs as the principal difference from cylindrite, which has two atomic layers thick Q slabs according to Makovicky (1974). They suggested that incaite should have the same structure. At least a partial structure study was necessary because, as demonstrated by Williams and Hyde (1988), the four-layer model cannot be selected from among other possible models based on purely metric differences of franckeite and cylindrite. As for the problem of incaite, we can suggest that the original electron microprobe data obtained by Makovicky (1974) from thin replacement shells of "incaite" in the cylinders of cylindrite might have been influenced by remnants of original cylindrite in these shells although none were detected by X-ray diffraction or, alternatively, the early electron-microprobe correction programs had problems with compositions combining heavy and light elements.

The interpretation based on two component lattices became standard in all subsequent works on franckeite, and they were

Table 1 Selection of published unit-cell data for franckeite

Compound	Q component	H component	Coincidence data	Reference
"Incaite"	$a = 5.79$ Å	$a = 3.66$ Å	along [010]	Makovicky (1976)
$FePb_{3.3}Ag_{0.3}Sn_{3.6}Sb_2S_{13}$	$b = 5.83$ Å	$b = 6.35$ Å	2×34.98 Å$_Q$ with	
	$c = 17.29$ Å	$c = 17.25$ Å	69.85 Å$_H$	
	$\alpha = 94.14°$	$\alpha = 91.13°$	12Q:11H	
	$\beta = 90°$	$\beta = 90°$		
	$\gamma = 90°$	$\gamma = 90°$		
	*A*2, *Am*, or *A*2/*m*	*A*2, *Am*, or *A*2/*m*		
"Potosiite"	$a = 5.84$ Å	$a = 3.70$ Å	along [010]	Wolf et al. (1981)
$Pb_{24.0}Ag_{0.2}Sn_{8.8}Sb_{7.8}Fe_{3.7}S_{55.6}$	$b = 5.88$ Å	$b = 6.26$ Å	188.06 Å	
	$c = 17.28$ Å	$c = 17.28$ Å	about 32Q:30H	
	$\alpha = 92.2°$	$\alpha = 92.2°$		
	$\beta = 90°$	$\beta = 90°$		
	$\gamma = 90°$	$\gamma = 90°$		
	*A*1 or $A\bar{1}$	*A*1 or $A\bar{1}$		
Franckeite (natural)	$a = 5.84$ Å	$a = 3.68$ Å	16Q:15H	Wang (1989)
	$b = 5.90$ Å	$b = 6.32$ Å		
	$c = 17.3$ Å	$c = 17.3$ Å		
	$\alpha = 95°$	$\alpha = 96°$		
	$\beta = 88°$	$\beta = 88°$		
	$\gamma = 91°$	$\gamma = 91°$		
Franckeite (natural)	$a = 5.82$ Å	$a = 3.62$ Å	16Q:15H	Wang (1988)
	$b = 5.92$ Å	$b = 6.30$ Å		
	$c = 17.5$ Å	$c = 17.5$ Å		
	$\alpha = 95.46°$	$\alpha = 95°$		
	$\beta = 91.46°$	$\beta = 90°$		
	$\gamma = 90°$	$\gamma = 90°$		
	A-centered	*A*-centered		
Franckeite	$a = 5.815$ Å	$a = 3.672$ Å	along [010]	present work
	$b = 5.873$ Å	$b = 6.275$ Å	modulation 45.80 Å	
	$c = 17.366$ Å	$c = 17.447$ Å	match	
	$\alpha = 94.98$ Å	$\alpha = 95.26°$	15.5Q:14.5H	
	$\beta = 88.43°$	$\beta = 95.45°$	at 91.1 Å	
	$\gamma = 89.97°$	$\gamma = 89.97°$		
	A-centered	*A*-centered		
Coiraite	$a = 5.862$ Å	$a = 3.660$ Å	14Q:13H	Paar et al. (2008)
$(Pb,Sn)_{12.5}As_3Sn_5FeS_{28}$	$b = 5.839$ Å	$b = 6.278$ Å		
	$c = 17.324$ Å	$c = 17.347$ Å		
	$\beta = 94.073°$	$\beta = 91.416°$		
	*P*2/*m*	*Am*		

Note: Only the sources containing a full set of lattice data are quoted; i.e., 2D-electron diffraction observations are not included.

observed in detailed powder diffraction studies by Mozgova et al. (1976), Mozgova (1983), Shimizu et al. (1992), and others. The common modulation of the two component structures, already seen for "incaite", has been found by subsequent single-crystal investigations of "potosiite" (Wolf et al. 1981) and by electron-diffraction studies of franckeite (Wang 1989). The octuple *b* parameter given for franckeite by Coulon et al. (1961) has been explained by Mozgova et al. (1976) as a misinterpretation of reflections of the unrecognized pseudohexagonal component. Table 1 quotes only complete determinations of lattice geometry of franckeite; selected partial determinations from electron diffraction studies are quoted in Makovicky and Hyde (1992).

The HRTEM studies connected with electron diffraction studies confirmed the kinship of cylindrite and franckeite and also demonstrated the apparent absence of a member with three atomic layers thick Q slabs or members with multiple H layers. Williams and Hyde (1988) state that "in franckeite the Q layer is twice as thick and the H layer the same thickness as in cylindrite, the former being PbS- or SnS-type, probably the latter. Similar corrugations parallel the vernier direction..." Their simulation tests for selecting one of these two layer types for the Q slab remained inconclusive. Interpretation of HRTEM data for "potosiite" by Kissin and Owens (1986) was discredited by Williams and Hyde (1988). Based on HRTEM studies, Wang (1989) and Wang and Kuo (1991) arrived at a four-layer model of the Q slab in the crystal structure of franckeite as well although their drawings appear schematic and the interlayer match suggested might be problematic. Ma et al. (1997) and Huang et al. (1986) adopted the model of franckeite proposed by Wang and Kuo (1991).

Interestingly, both Ma et al. (1997) and Henriksen et al. (2002) observed only pseudohexagonal surface motifs on freshly cleaved surfaces of franckeite by STM and AFM; the pseudotetragonal motifs were missing. In AFM, the H surface appears in full agreement with crystallographic studies. Pattern observed in the STM images by Henriksen et al. (2002) is a $\sqrt{3} \times \sqrt{3}$ orthohexagonal superstructure formed on imaging because specific atomic sites of the surface layer are less conductive. Ma et al. (1997) observed a 47 Å sinusoidal modulation wave, whereas Henriksen et al. (2002) found layer modulation wavelengths of 36.5–38.5, 40.0–42.0, and 43.5–45.5 Å, corresponding to the Q/H interlayer matches of 13/12, 14/13, and 15/14 subcells, respectively. They did not find the match of 16Q/15H reported by Wang (1989) and Wolf et al. (1981). The different match ratios correlate probably with different Pb/Sn^{2+} ratios; they occurred in different areas of a rather small single flake of franckeite.

Previous compositional studies

The complex composition and crystallography of franckeite is reflected in a plethora of approaches and resulting chemical formulas for this "mineral species" or, more exactly, for this variable-fit series (for definition see Makovicky 1997, 2005) of closely related phases with slightly different interlayer matches. The first chemical formulas of franckeite from Poopo, Bolivia, $Pb_5Sn_3Sb_2FeS_{14}$ and $Pb_{4.5}Sn_{2.5}Sb_2FeS_{13}$,were suggested by Prior (1904) for two different specimens analyzed. Ahlfeld and Moritz (1933) proposed an iron-free formula, $Pb_5Sn_3Sb_2S_{14}$ and various iron-free formulas found subsequently their way into many handbooks, e.g., Strunz (1977). Syntheses by Sachdev and Chang (1975), Moh (unpublished, quoted by Li), and Li (1984) show, however, that neither cylindrite nor franckeite form without iron. The only suggestion to the contrary comes from the hydrothermal syntheses by Nekrasov et al. (1975), but the nature of the products they obtained should be reinvestigated. Microprobe analyses of franckeite samples from Bolivia, China, Canada, and Siberia by Bernhardt (1984) resulted in a formula

$$(Pb^{2+}_{w}, Ag^{+}_{x})_{\Sigma=6-y}Sn^{2+}_{y-x+z/2}Sn^{4+}_{2+z/2}Sb^{3+}_{2+x-z}(Fe^{2+},Zn^{2+})S^{2-}_{14}$$

with approximate values

w = 4–6, x = 0–0.5, y = 0–2, z = 0.1–0.5.

Paar et al. (2008) described an arsenian analog of franckeite, named coiraite, with idealized formula $(Pb, Sn)_{12.5}As_3Sn_5FeS_{28}$, with a heavily plumbian Q component. The published X-ray data obtained from a combination of electron microdiffraction and powder diffraction data refinement are in Table 1.

The combined dry syntheses at 600 °C and hydrothermal syntheses at 300 and 250 °C and 600 bars by Li (1984) and Moh and Li (1986) yielded a field of franckeite limited by the Pb-rich compositions $Pb_5FeSb_2Sn_2S_{13}$–$Pb_6FeSb_2Sn_2S_{14}$ and reaching possibly the lead-free composition $Sn_6FeSb_2Sn_2S_{14}$.The formula derived is $(Pb,Sn)^{2+}_{6-x}Fe^{2+}Sb^{3+}_2Sn^{4+}_2S_{14-x}$ with $(0 \le x \le 1)$. These syntheses were accompanied by X-ray powder diffraction but not by electron microprobe analyses. Minor Ag was added in the syntheses by Li (1989). Shimizu et al. (1992) indicated $Pb_6FeSb_2Sn_2S_{14}$ and $(Sn^{2+}, Pb)_{6+x}Fe^{2+}Sb^{3+}Sn^{4+}_2S_{14+x}$ where $Sn^{2+} >$ Pb and x ~ 2. Chemical formulas of cylindrite and franckeite from several specimens in the work of Mozgova et al. (1977) are based on two Sb atoms pfu. Potosiite was defined by Wolf et al. (1981) as $4PbS.22SnS_2.7FeS.9Sb_2S_3$. The chemical formulas used in all these works are pure stoichiometric ones, without a reference to crystal structure. Makovicky (1974) gives a formula normalized to 100 cations pfu but also a structure-based formula for a coincidence mesh of a Q-H layer pair.

Organova et al. (1980) suggested a schematic formula MeS.$k$$MeS_2$ for cylindrite and 2MeS·$k$$MeS_2$ for franckeite, with k equal to the ratio of areas of the two cells, a pseudotetragonal cell and a pseudohexagonal cell, in the (001) plane [our notation], i.e., $k = (area)_Q/(area)_H$. Organova et al. (1980) state that the variation of k is rather limited. In partial agreement with this formula, Mozgova (1983) describes the franckeites studied by a group formula

$$2[(Pb+Ag+Sn^{2+})_{18+0.25x}(Sb+Fe)_{6-0.25x}]_{24}$$
$$S_{24}\cdot 1.56(Sn^{4+}_{7.5}Sb_{2.1}Fe_{1.4})_{11}S_{22}.$$

Coefficient x varies from 1 to 3 in normal franckeite and between 4 and 9 in "low-antimony" high-Pb franckeite. The formula calculation by Mozgova (1983) was undertaken using the 12Q:11H cell match from "incaite" instead of the match of cells in a particular specimen, i.e., a general formula $2Me_{24}S_{24}\cdot 1.58Me_{11}S_{22}$ was used. Her approach disregards the changes in the Q:H match ratios that parallel the changes in the Pb/Sn^{2+} ratio.

Besides the question of changing Q:H area ratios, the standing problem of structure-based chemical formulas of the members of the cylindrite-franckeite family has been the distribution of iron and antimony between the Q and H layers and the valence

of iron in these compounds. Since the description of the structure of levyclaudite (Evain et al. 2006), in which Fe was "replaced" by two highly visible Cu^{+} atoms flanking the vacated Sn^{4+} octahedra of the H layer and not placed centrally in them as the iron atoms are, iron has been placed in the H layers and, partly as a consequence, Sb has been confined to the Q layers.

Published suggestions concerning the valence of iron and even those of antimony and tin in franckeite are rather contradictory. Pen'kov and Safin (1971) found Sb^{3+} "with axial symmetry" (i.e., with a pronounced SbS_3 signature) by means of nuclear quadrupole resonance. Manapov and Pen'kov (1976) found both Sn^{4+} and Sn^{2+} in franckeite, but the latter was present in much smaller amounts than the former. They found high-spin octahedral Fe^{2+} side by side with low-spin Fe^{2+} although they also mention admixture of marcasite, observed by reflected light microscopy, which could be responsible for the latter component. In his examination of synthetic products produced by Li (1984), Amthauer (1986) reports pure octahedrally coordinated Fe^{2+} in Sn-rich franckeite as well as in Pb-free franckeite. He states that if any other type of iron is present, it must be under 10%, i.e., below a detectability threshold. His Mössbauer studies indicated Sb^{3+} and simultaneous presence of Sn^{4+} and Sn^{2+}, in both in Pb-rich and Sn-rich franckeite varieties, and even in potosiite. Novikov (in Mozgova et al. 1975) found both types of iron in natural franckeite, stating that Fe^{3+} predominates. Wu and Huang (1986) found two types of Fe^{2+} in Pb-rich franckeite from Dachang and two types of Sn, which they describe as Sn^{4+}, suggesting that in both cases the two cation sites belong to the two types of layers. Smith and Zuckermann (1967) reported exclusive presence of Sn^{4+} in franckeite. Similarly, Hunger et al. (1986) found Sn^{4+}, Fe^{2+}, and Sb^{3+}, with small amounts of Sn^{2+} only in franckeite but not in "potosiite". Potosiite supposedly contains some Fe^{3+} and Sb^{5+}. Many of these statements appear to indicate insufficient sensitivity of especially older instruments or insufficient collection times (Pb is a strong absorber). Furthermore, results like those of Hunger et al. (1986) suggest to us undetected presence of minerals of the stannite family replacing cylindrite-franckeite, as already observed by Makovicky (1974).

Present investigation

Chemical analysis

The crystals of franckeite examined in this study were freed from a crust of franckeite crystals originating from San Jose, Bolivia, purchased from Gregorio Mamani, Oruro, Bolivia. Chemical analyses of franckeite from San José, Bolivia, were carried out by means of an electron microprobe apparatus at the University of Salzburg. The JEOL JXA-8600 (Probe for Windows) apparatus in WDS mode was used. The experimental conditions were as follows: acceleration voltage 25 kV; beam current 30 nA; beam diameter 3 μm; correction procedure: on-line ZAF correction. Standards used are as follows: Ag metal (synth.) Ag$L\alpha$, galena (nat.) Pb$L\alpha$, Bi_2Se_3 (synth.) Bi$L\alpha$, stibnite (nat.) Sb$L\alpha$ and S$K\alpha$, Bi_2Se_3 (synth.), and Sn metal (synth.) Sn$L\alpha$. Selenium was not detected.

Fifteen microprobe analyses of franckeite from San Jose, Bolivia, gave 50.14(15) wt% Pb (range 49.74–50.35 wt%), 0.77(4) wt% Ag (0.71–0.84 wt%), 0.02(2) wt% Cu (0.00–0.05 wt%), 2.60(5) wt% Fe (2.53–2.69 wt%), 13.06(9) wt% Sn (12.92–13.22 wt%), 12.45 wt% Sb (12.26–12.86 wt%), and 21.49(16) wt% S (21.24–21.77 wt%). Total 100.53 wt% (range 100.01–100.93 wt%). For 100 atomic percent, they result in a formula $Pb_{20.54(11)}Ag_{0.60(3)}Cu_{0.03(2)}Fe_{3.95(8)}Sn_{9.34(7)}Sb_{8.68(12)}S_{56.87(23)}$ (parentheses contain standard deviations in terms of the last digit). With Ag+Cu plus an equivalent portion of Sb recalculated to 2Pb, they result in a simplified formula $Pb_{21.74}Sn_{9.34}Fe_{3.95}Sb_{8.08}S_{56.87}$.

X-ray crystallography: Experimental methods

About 20 crystals were tried, among which only two were found of quality suitable for X-ray diffraction and used. The problem is the universally present contortion of soft tabular franckeite crystals (Fig. 1). Specification of collection and processing conditions of X-ray diffraction data are in Table 2.

The samples were tested on the Oxford Diffraction Xcalibur diffractometer and in all of them twinning with a twofold axis along the **b** direction (see below) acting as a twin axis has been detected. This leads to overlapping of diffraction spots expressed by the twinning matrix

$$\begin{bmatrix} h_T & k_T & l_T \end{bmatrix} = \begin{bmatrix} h & k & l \end{bmatrix} \cdot \begin{bmatrix} -1 & 0 & 0 \\ 0 & 1 & -1/2 \\ 0 & 0 & -1 \end{bmatrix}$$

This made the process of integration difficult especially because the above relationship is to be applied both to the main reflections and to the satellites with generally non-integral values. Some diffraction spots were separated, some were completely overlapped, and some were partly overlapped. The partly overlapped reflections could not be correctly integrated, and therefore we had to exclude them from the refinement. Nevertheless more than 91% of reflections were finally processed into the refinement.

Intensities were integrated and corrected for LP and absorption by means of the CrysAlis CCD program (Oxford Diffraction 2009). Structure calculations were performed by the JANA2006 package (Petříček et al. 2006). Initial configurations were determined by a charge-flipping program Superflip (Palatinus and Chapuis 2007) for each component and then amalgamated. General description of the principles and procedures of the modulated structure refinement are given in the reviews published by van Smaalen (1995), Janssen et al. (1999), Petříček and Coppens (1985, 1988), and Petříček et al. (1991).

Figure 1. Crystals of franckeite from San Jose mine, Bolivia. Note the excellent (001) cleavage and pliable character of the mineral. SEM photograph.

TABLE 2. Crystal data, experimental, and refinement parameters

Crystal data		
Temperature	300 K	
Chemical formula	$[Fe_{0.431}\ Sn_{0.569}\ S_2][Pb_{1.352}(Sb/Sn)_{1.345}\ S_{2.697}]$	
Superspace group	$C\bar{1}(\sigma_{11},\sigma_{12},\sigma_{13},\sigma_{21},\sigma_{22},\sigma_{23})$	
Cell parameters		
(centered cell):	H – $[Fe_{0.431}\ Sn_{0.569}\ S_2]$, ν = 1	Q – $Pb_{1.352}(Sb/Sn)_{1.345}\ S_{2.697}$, ν = 2
$a_{\nu 1}$ (Å)	3.665(8)	5.805(8)
$a_{\nu 2}$ (Å)	6.2575(16)	5.856(16)
$a_{\nu 3}$ (Å)	17.419(5)	17.338(5)
α_ν (°)	95.25(2)	94.97(2)
β_ν (°)	95.45(2)	88.45(2)
γ_ν (°)	89.97(2)	89.94(2)
V_ν (Å^3)	398.47(18)	587.0(2)
$\mathbf{q}_{\nu 1}$	$-0.00087(8)\ \mathbf{a}^*_{11} + 0.13725(16)\ \mathbf{a}^*_{12} - 0.0314(4)\ \mathbf{a}^*_{13}$	$-0.00129(8)\ \mathbf{a}^*_{21} + 0.128436(10)\ \mathbf{a}^*_{22} - 0.0299(3)\ \mathbf{a}^*_{23}$
Z	2	
Density, calc (g/cm^3)	8.9802	
Crystal color	Gray	
Crystal shape	Plate	
Crystal size (mm)	0.25 × 0.16 × 0.03	
Data collection		
Diffractometer	XCalibur CCD, Oxford Diffraction	
Radiation	Mo K-$L_{2,3}$ (0.71069 Å)	
Monochromator	oriented graphite (002)	
Scan mode	ω	
θ_{max} (°)	26.55	
hklmn range	$-4 \le h \le 4$ $-10 \le k \le 10$ $-22 \le l \le 22$ $-8 \le m \le 8$ $-7 \le n \le 7$	
No. of reflections	61074	
Data reduction		
Linear abs. coeff. (mm^{-1})	59.24	
Absorption correction	Analytical method	
T_{min}/T_{max}	0.013/0.363	
No. of independent refl.	8977	
Criterion for obs.	$I \ge 3\sigma(I)$	
No. of observed refl.	7397	
R_{int} (obs)	0.0861	
Refinement		
Refinement coefficient	F	
F(000)	587	
No. of refined parameters	170	
Weighting scheme	$w = 1/[\sigma_2\lvert F_{obs}\rvert + (0.01\lvert F^o\rvert)_2]$	
R/Rw	see Table 3	
S (obs)	3.48	
Diff. Fourier (e$^-$/Å$_3$)	[–4.27, 4.68]	

SUPERSPACE DESCRIPTION

Franckeite is a two-dimensionally incommensurate structure with intense one-dimensional modulation. Along the latter direction, satellites reach high orders. The overall intensity distribution reflects a transverse sinusoidal modulation of the entire structure, similar to theoretical models of Korekawa (1968). We have altered the hitherto used orientation of crystallographic axes to conform to the ample literature on layer-misfit compounds (Wiegers and Meerschaut 1992; Makovicky and Hyde 1992). Thus, the **a** and **b** directions will be parallel to the layers; the new **a** direction corresponds to the old unmodulated **b** direction and the new **b** direction is the direction exhibiting common layer modulation (corresponding to the old **c** direction defined for franckeite by, e.g., Makovicky and Hyde 1981, 1992). In the new notation, **c** is the layer-stacking direction. The transformation matrix from the old notation is (010/001/100). The choice of *C*-centered cells [in the present orientation] was made already by Makovicky (1974) for similar component lattices of cylindrite because of the simple relationships (i.e., parallelism of respective **a** and **b** vectors) between the fundamental directions of the two components.

Both cells have the γ angle practically equal to 90° (Table 2). The α angles of both cells are nearly equal, ~ 95°, whereas the β angles display a principal difference: 95.45° for the H component and 88.43° for the Q component. This is a reversal of the situation in the synthetic Sn-Se cylindrite (Makovicky et al. 2008) where these angles are 90.59° and 83.14° in the same order of components. Thus, the **c** lattice vectors of the two components diverge considerably, whereas their $\mathbf{a} \times \mathbf{b}$ planes coincide. Therefore, the two reciprocal lattice components, the pseudotetragonal Q component and the pseudohexagonal H component, have one reciprocal axis, $\mathbf{a}^*_{13} = \mathbf{a}^*_{23}$, and the modulation vector, $\mathbf{q}_1 = \mathbf{q}_2$, in common. In this refinement, the pseudohexagonal H subsystem is "system 1", whereas the pseudotetragonal Q subsystem is "system 2". The second subscript in the above and following symbols indicates the **a**, **b**, and **c** axes of the given subsystem, in this order.

With the pseudohexagonal subsystem 1 as a reference system, the first three vectors of the higher-dimensional lattice are $\mathbf{a}^*_{11}$, $\mathbf{a}^*_{12}$, $\mathbf{a}^*_{13}$, whereas $\mathbf{a}^*_4 = \mathbf{q}_1$ and $\mathbf{a}^*_5 = ½\ (\mathbf{a}^*_{21} + \mathbf{a}^*_{22})$.

We obtain the same (3+2) vector system as was used by Makovicky et al. (2008) for synthetic cylindrite.

The components of the σ matrix (van Smaalen 1995) are defined as

$$\begin{pmatrix} \mathbf{q}_{11} = \mathbf{a}^*_{14} \\ \mathbf{q}_{12} = \mathbf{a}^*_{15} \end{pmatrix} = \sigma \begin{pmatrix} \mathbf{a}^*_{11} \\ \mathbf{a}^*_{12} \\ \mathbf{a}^*_{13} \end{pmatrix}$$

$$\sigma = \begin{pmatrix} -0.00087 & 0.13725 & -0.0314 \\ 0.6309 & 1.0688 & -0.3815 \end{pmatrix}$$

and the W^2 matrix, which ties the second reference (Q) subsystem to the first (H) one

$$W^2 = \begin{bmatrix} 0 & -1 & 0 & -1/2 & 1 \\ 0 & 1 & 0 & 1/2 & 0 \\ 0 & 0 & 1 & 0 & 0 \\ 0 & 0 & 0 & 1 & 0 \\ 1 & 1 & 0 & 0 & 0 \end{bmatrix}$$

The (001) planes (i.e., orientations of the respective $\mathbf{a}^*_{\nu,3}$ axes, ν = 1, 2) of both components coincide. The small deviation of the **q** vector from the $\mathbf{a}^*_{\nu,1} \times \mathbf{a}^*_{\nu,2}$ planes is significant and calculations indicate that, within measurement accuracy, the wave normal of the modulation wave lies in the (001) plane and wave fronts are perpendicular to (001) (in new notation).The modulation vector (wave normal) in direct space is

$$-0.132\ \mathbf{a}_{11} + 7.290\ \mathbf{a}_{12} + 0.022\ \mathbf{a}_{13}$$
$$-0.090\ \mathbf{a}_{21} + 7.790\ \mathbf{a}_{22} + 0.022\ \mathbf{a}_{23}$$

i.e., it is parallel to the **b** direction and identical for both components (H and Q, respectively). It is equal to ~45.9 Å. Similar

to cylindrite (Makovicky 1974; Makovicky et al. 2008), the layer-stacking directions $\mathbf{a}_{\nu,3}$ are oblique to the (001) plane, as indicated by the respective α and β angles.

Structure refinement

Initial atom coordinates were obtained from Superflip (Palatinus and Chapuis 2007). The two subsystems were first refined separately, before being joined in a common (3+2)-dimensional refinement.

The modulation wave for a position parameter i of an atom μ of a subsystem ν is defined as:

$$x_{\nu i}^{\mu}\left(x_4,x_5\right)=x_{\nu i,0}^{\mu}+\sum_{n_1,n_2}^{\infty}x_{i,s,n_1,n_2}^{\mu}\sin\left[2\pi\left(n_1x_{\upsilon 4}+n_2x_{\upsilon 5}\right)\right]+$$
$$\sum_{n_1,n_2}^{\infty}x_{i,c,n_1,n_2}^{\mu}\cos\left[2\pi\left(n_1x_{\upsilon 4}+n_2x_{\upsilon 5}\right)\right]$$

Coordinates of an atom μ refer to the unit cell of its own subsystem.

In a similar way, the modulation wave for occupational parameter of an atom μ of a subsystem ν is defined as:

$$o_{\upsilon}^{\mu}\left(x_4,x_5\right)=o_{\nu,0}^{\mu}+\sum_{n_1,n_2}^{\infty}o_{s,n_1,n_2}^{\mu}\sin\left[2\pi\left(n_1x_{\upsilon 4}+n_2x_{\upsilon 5}\right)\right]+$$
$$\sum_{n_1,n_2}^{\infty}o_{c,n_1,n_2}^{\mu}\cos\left[2\pi\left(n_1x_{\upsilon 4}+n_2x_{\upsilon 5}\right)\right]$$

Refinement conditions are summarized in Tables 2 and 3, and refinement results for the positional and occupational modulation waves are given in Tables 4 and 5, respectively. The anisotropic displacement parameters (Table 6) were not modulated. The H subsystem has just two "atoms" Sn/Fe1 and S1 (each "atom" is an array of atoms with positions modulated from an average x, y, z coordinate by means of sine and cosine modulation waves); the Q subsystem has two cations, Pb/(Sn,Sb)2 and Pb/(Sn,Sb)3. (In the process of the refinement they were represented by Pb and Sn, as given in the tables; in the text they will be referred to as Pb2 and Pb3 for brevity.) The Q subsystem also has two anions, S2 and S3. Both reveal pronounced transverse modulation waves, with the amplitudes directed along the $\mathbf{a}_{\nu,3}$ direction (Fig. 2).The $z$sin1 and $y$cos1 functions are by far the largest contributors, i.e., the modulation is close to a sinusoidal modulation of a semi-rigid layer. There is a slight linearization of the sloping portions of the Q modulation wave, expressed as a very minor contribution of higher-order waves (Table 4). The amplitude of the transverse z-modulation is ~0.75 Å for Pb2, the cation on the surface of the Q slabs, and ~0.72 Å for the Sn1 cation in the H layer.

There is a near-zero y-modulation for the cation in the H layer (Fig. 3), but both the cations and anions of the Q slab display important longitudinal y-modulation wave with a phase shift of 1/4 to 1/6 $\lambda_{\text{modulation wave}}$ against the z-modulation (Figs. 4 and 5). This is explained as the movement of atoms on both sides of the median plane of a fairly rigid Q slab that takes place when this 4 atomic layers thick slab is bent, being near-sinusoidally modulated. Atoms situated around inflection points move along the z- and y-directions as a part of a stiff body, whereas those closest to the convex maximum and concave minimum of the sinusoidal wave undergo only stretching or compression of intralayer interatomic distances (facilitated by local changes in chemistry that are discussed below). The y component is smaller for Pb3 and for the S3 atom situated in the interior of the Q layer because

TABLE 3. Residual factors* for the (3+2)-dimensional superspace refinement of franckeite

Reflection subset	No. of reflections (obs)	$R(F)/Rw(F)$
All	7396	0.0935/0.0823
Main	1155	0.0815/0.0746
First order	2448	0.0857/0.0766
Second order	2079	0.0955/0.0858
Third order	1239	0.1136/0.1034
Fourth order	475	0.1688/0.1759

* R factors defined as:
$R=\Sigma||F_{obs}|-|F_{calc}||/\Sigma|F_{obs}|$
$Rw=(\Sigma w||F_{obs}|-|F_{calc}|)^2/\Sigma w|F_{obs}|^2)^{1/2}$.

TABLE 4. Positional modulation parameters for franckeite

Atom (μ)	ν	Occupancy	Wave	x	y	z	U_{eq}
Sn1/Fe1	1	0.57(2)/		0.25	0.25	0	0.0259(5)
		0.43(2)	s,1,0	–0.0196(6)	–0.0106(3)	–0.04020(13)	
			c,1,0	0	0	0	
			s,0,1	0	0	0	
			c,0,1	0	0	0	
			s,2,0	–0.0015(13)	–0.0046(3)	–0.00024(19)	
			c,2,0	0	0	0	
			s,3,0	0.0027(14)	0.0026(5)	0.00154(17)	
			c,3,0	0	0	0	
S1	1	1		0.2882(11)	0.6070(4)	0.08270(18)	0.0468(15)
			s,1,0	–0.008(2)	–0.0082(6)	–0.0395(3)	
			c,1,0	0.0000(16)	0.0194(5)	0.0002(3)	
			s,0,1	0	0	0	
			c,0,1	0	0	0	
			s,2,0	0.001(3)	–0.0067(7)	0.0024(4)	
			c,2,0	0.004(3)	0.0015(8)	–0.0001(3)	
			s,3,0	–0.001(5)	–0.0031(9)	0.0014(4)	
			c,3,0	–0.001(3)	–0.0026(9)	0.0000(4)	
Pb2/Sn2	2	0.74(2)/		0.63901(12)	0.97083(10)	–0.23153(4)	0.0353(2)
		0.26(2)	s,1,0	0.00117(16)	–0.00665(14)	–0.04334(6)	
			c,1,0	–0.00433(16)	0.05204(13)	–0.00027(6)	
			s,0,1	0	0	0	
			c,0,1	0	0	0	
			s,2,0	–0.0012(2)	0.01064(14)	0.00023(7)	
			c,2,0	–0.00030(18)	0.00022(15)	0.00096(7)	
			s,3,0	–0.0002(2)	–0.00046(17)	0.00120(7)	
			c,3,0	0.0005(3)	–0.00290(16)	–0.00001(9)	
Pb3/Sn3	2	0.265(18)/		0.17797(15)	0.95073(13)	–0.41250(5)	0.0353(3)
		0.735(18)	s,1,0	0.0001(2)	–0.01110(18)	–0.04212(8)	
			c,1,0	–0.00434(20)	0.00984(15)	–0.00031(8)	
			s,0,1	0	0	0	
			c,0,1	0	0	0	
			s,2,0	–0.0015(2)	0.00292(16)	0.00007(9)	
			c,2,0	0.0006(2)	0.00104(16)	0.00055(8)	
			s,3,0	0.0006(3)	–0.0003(2)	0.00044(10)	
			c,3,0	0.0005(4)	0.0000(2)	0.00019(11)	
S2	2	1		0.1435(6)	0.9653(5)	–0.2660(2)	0.0354(12)
			s,1,0	–0.0016(8)	–0.0099(7)	–0.0435(3)	
			c,1,0	–0.0034(9)	0.0479(7)	–0.0011(4)	
			s,0,1	0	0	0	
			c,0,1	0	0	0	
			s,2,0	–0.0010(11)	0.0071(7)	0.0003(4)	
			c,2,0	0.0014(10)	0.0013(8)	0.0019(4)	
			s,3,0	0.0011(13)	0.0004(9)	0.0022(4)	
			c,3,0	0.0010(15)	–0.0056(8)	–0.0005(5)	
S3	2	1		0.1349(9)	1.4239(8)	–0.4040(2)	0.0556(16)
			s,1,0	–0.0033(11)	–0.0090(11)	–0.0439(4)	
			c,1,0	–0.0052(12)	0.0145(10)	0.0002(4)	
			s,0,1	0	0	0	
			c,0,1	0	0	0	
			s,2,0	–0.0057(15)	0.0059(10)	–0.0005(4)	
			c,2,0	0.0005(13)	0.0011(10)	0.0012(4)	
			s,3,0	–0.0023(18)	0.0012(14)	0.0011(4)	
			c,3,0	–0.005(2)	0.0000(14)	–0.0005(5)	

TABLE 5. Occupational modulation parameters for franckeite

Atom (μ)	ν	Occupancy	Wave	Occupational wave
Sn1	1	0.57(2)		
			s,1,0	0
			c,1,0	–0.007(8)
			s,0,1	0
			c,0,1	0
			s,2,0	0
			c,2,0	0.045(10)
			s,3,0	0
			c,3,0	–0.008(15)
Pb2	2	0.74(2)		
			s,1,0	–0.091(4)
			c,1,0	0.002(5)
			s,0,1	0
			c,0,1	0
			s,2,0	–0.005(6)
			c,2,0	0.140(5)
			s,3,0	0.085(6)
			c,3,0	–0.001(7)
Pb3	2	0.265(18)		
			s,1,0	–0.085(4)
			c,1,0	0.001(4)
			s,0,1	0
			c,0,1	0
			s,2,0	0.010(5)
			c,2,0	0.055(5)
			s,3,0	0.040(6)
			c,3,0	–0.005(7)

Note: Occupancy of Fe1, Sn2, and Sn 3 is equal to 1 minus occupancy of Sn1, Pb2, and Pb3, respectively. Modulation wave coefficients of Fe1, Sn2, and Sn3 have the same numerical values as the respective coefficients for Sn1, Pb2, and Pb3 *but with opposite signs.*

TABLE 6. ADP harmonic parameters for franckeite

Atom	ν	U^{11}	U^{22}	U^{33}	U^{12}	U^{13}	U^{23}
Sn1/Fe1	1	0.0357(10)	0.0082(5)	0.0344(11)	0.0004(6)	0.0082(7)	0.0005(6)
S1	1	0.090(4)	0.0156(11)	0.035(2)	0.0010(13)	0.006(2)	0.0007(12)
Pb2/Sn2	2	0.0269(4)	0.0301(3)	0.0484(5)	–0.0008(2)	0.0000(3)	0.0010(3)
Pb3/Sn3	2	0.0300(6)	0.0314(4)	0.0443(7)	0.0077(3)	0.0057(4)	0.0051(3)
S2	2	0.0207(18)	0.0236(13)	0.061(3)	0.0028(12)	0.0043(15)	0.0025(14)
S3	2	0.058(3)	0.074(3)	0.033(2)	–0.028(2)	0.0047(19)	–0.005(2)

they are closer to the median plane (Figs. 6 and 7). Occupancies of the mixed cation positions Pb2 [the "outer" cation of the Q slab, average occupancy refined as 0.74(2) Pb, rest being Sn/Sb)] and Pb3 [the "inner" cation of the Q layer, average occupancy refined as 0.27(2) Pb, and 0.73(2) Sb/Sn] display a substantial and complicated modification (Fig. 8); important contributions to its modeling are made by the functions of up to the third order (Table 5). Compositional modulation of the Sn/Fe1 position in the H layer is much less pronounced (Fig. 9).

The (3+2)-dimensional refinement of the franckeite structure included satellites up to fourth order. Number of reflections included and the respective resulting $R(F)$ and $R_w(F)$ agreement factors are in Table 3.

DESCRIPTION OF THE STRUCTURE

Principal features

The crystal structure of franckeite consists of pseudotetragonal Q slabs that are four atomic layers thick alternating with single-octahedron pseudohexagonal H layers (Fig. 2). Cation coordinations and refinement results suggest that the Q slabs contain all of Pb, as well as Sn^{2+}. In the structure refinement, the latter cannot be distinguished from the Sb^{3+} contents indicated by the chemical analysis because of similar atomic number and coordination. The H layer indicates presence of Sn^{4+} mixed

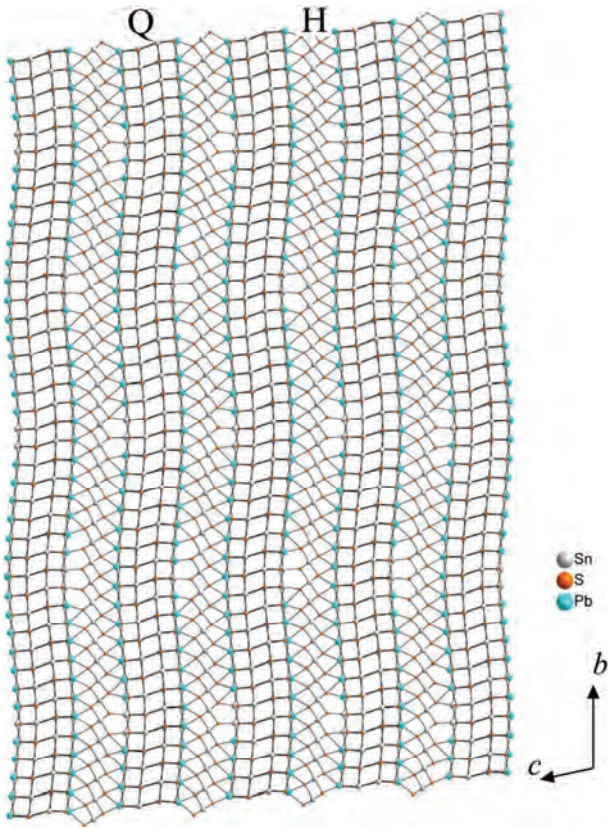

FIGURE 2. The crystal structure of franckeite projected along [100]. Four atomic layers thick pseudotetragonal Q slabs alternate with single-octahedron pseudohexagonal H slabs. Both display a notable positional transversal modulation along the c direction and a non-commensurate contact between the two types of slabs. Long cation-anion distances between the Q and H slabs and in the interior plane of the Q slabs have been drawn to accentuate the modular relationships between different components of the structure.

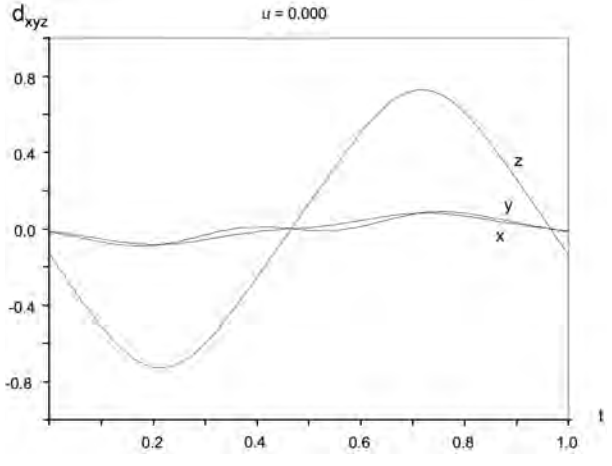

FIGURE 3. Positional modulation for the octahedrally coordinated (Sn, Fe) position labeled as Sn1 in the H layers of franckeite. Deviations (in angstroms) along the three axes, *x*, *y*, and *z* are plotted against the modulation parameter *t*. There is no modulation along the parameter *u*.

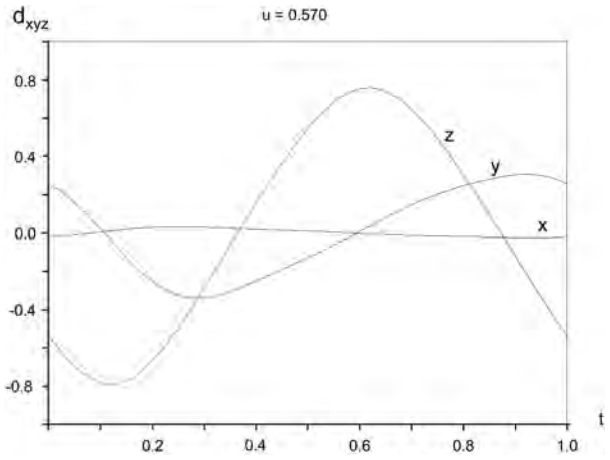

FIGURE 4. Positional modulation for Pb2 in the surface of the Q slabs of franckeite. Deviations (in angstroms) along the three axes, *x*, *y*, and *z* are plotted against the modulation parameter *t*. There is no modulation along the parameter *u*. Out-of-phase shift of the *y* curve is discussed in the text.

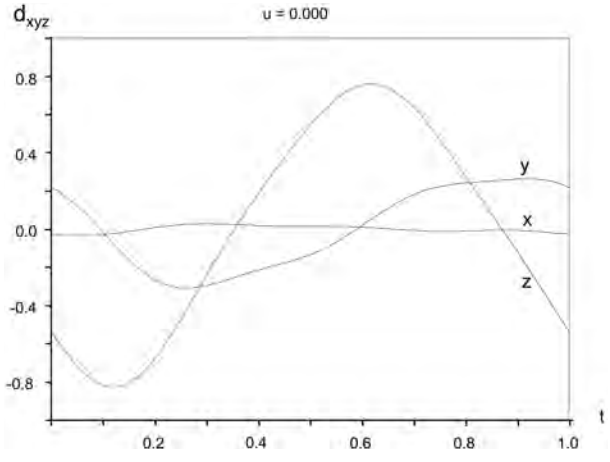

FIGURE 5. Positional modulation for S2 from the surface of the Q slabs of franckeite. For details see Figure 4.

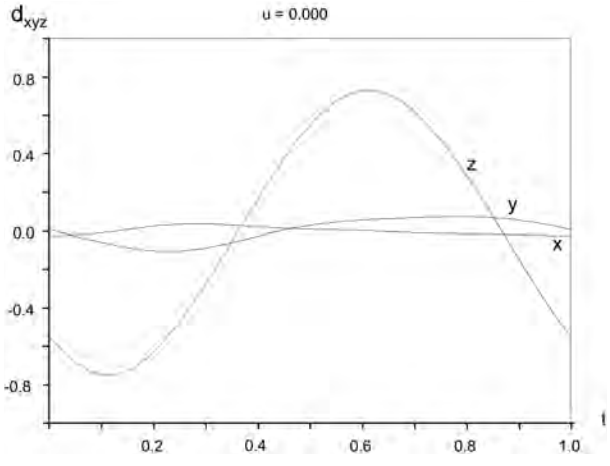

FIGURE 6. Positional modulation for the mixed cation position labeled as Pb3 in the interior atomic planes of the Q slab. For details see Figure 4.

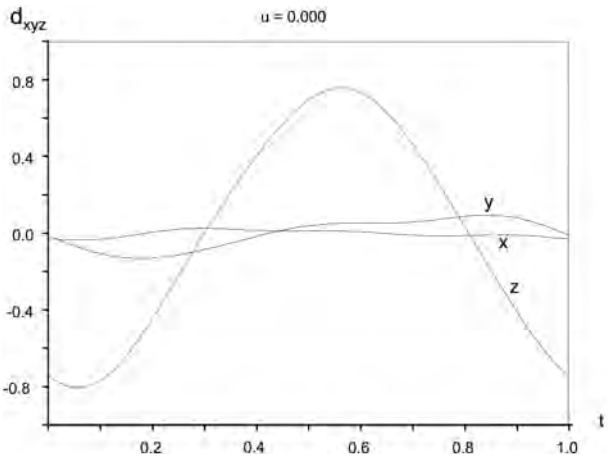

FIGURE 7. Positional modulation for S3 in the interior atomic planes of the Q slab. For details see Figure 4.

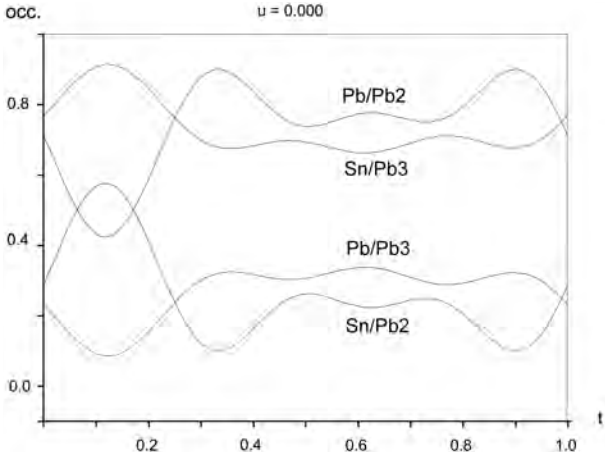

FIGURE 8. Occupational modulation of the Pb2 and "Pb3" positions in the Q slab, expressed as the percentage of Pb and Sn, respectively. Top curves: Pb in Pb2 with a pronounced minimum in the region that has maximum *z* deviation and (Sb, Sn) in Pb3 with a modest maximum in this region. Bottom curves: Sn in the Pb2 site with a pronounced maximum and Pb in Pb3 with a modest minimum in the maximally displaced slab portions. Note the flat character of all curves in the regions surrounding the inflection points. For correlation, identical abscissa is used as in Figure 4. Antimony is included as a part of Sn in the refinement.

with iron; no coordinations ascribable unambiguously to Sb^{3+} were observed. Periodicities of the two layers differ in the **a** direction, being 3.665(8) and 5.805(8) Å, respectively, without detectable modulation. In the modulated **b** direction, the match of $\mathbf{b}_H$ equal to 6.2575(16) Å with $\mathbf{b}_Q$ equal to 5.856(16) Å is closest to a combination of 15 H with 16 Q cells [both are *C*-centered] (93.86 Å matching 93.70 Å, a mismatch of only –0.17 Å); this combination lies in the range of matches discussed in the literature (quoted above) for the cylindrite-franckeite series and is in agreement with its Pb-rich composition. The next closest match is 14 H cells with 15 Q cells, 87.61 vs. 87.84 Å, with a mismatch of +0.24 Å, i.e., the true match mode might be 14.5 H

cells with 15.5 Q cells, with the average match length of 90.75 Å and error of only 0.034 Å, as also assumed in the example that follows below. The b_H/b_Q ratio is 1.0686. The latter match length corresponds to 1.989 times the length of the modulation vector equal to 45.617 Å, creating a difference of about –0.24 Å for each ~91 Å period. A cumulative effect of this difference between the match propagation and modulation length over a sum of consecutive modulation periods is important for the crystallography of franckeite.

For comparison, another less perfect crystal from the same sample had a = 5.815 Å, b = 5.873 Å, c = 17.366 Å, α = 94.98°, β = 88.43°, γ = 89.97°; the modulation vector **q** = –0.001 **a*** + 0.1282 **b*** – 0.0295 **c*** for the Q component and a = 3.672 Å, b = 6.275 Å, c = 17.447 Å, α = 95.26°, β = 95.45°, γ = 89.97°; the modulation vector **q** = –0.001 **a*** + 0.1374 **b*** – 0.031 **c*** for the H component. For this sample, the match of centered cells in this **b** direction is again 15.5 Q:14.5 H (ratio 1.069), at 91.01 Å. This value is a double of the modulation vector minus a structurally important difference Δ = 0.59 Å. The length of the wave derived from the modulation vector is 45.80 Å. These data indicate that the heterogeneity of the present sample is more limited than the one reported for franckeite by Henriksen et al. (2002). All these empirical values depend critically on the quality of data that can be derived from the natural material examined.

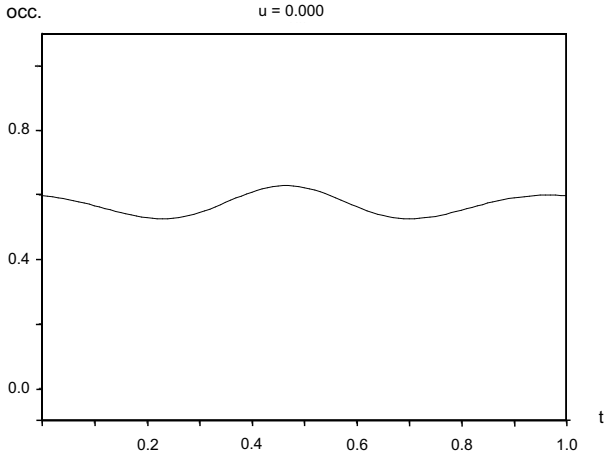

FIGURE 9. Modulation of the occupancy parameter of the octahedrally coordinated Sn1 site in the H layers (expressed as a fraction of the value for pure Sn) along the parameter t. For correlation, identical abscissa is used also in Figures 3 and 11. Lowest occupancy values (i.e., highest contents of Fe) occur for the largest values of z deviations.

A specific feature of franckeite is a well-defined space for non-bonding electrons of the inner Q cations (which is the central space of a lone electron pair micelle, Makovicky and Mumme 1983) situated between the two inner cation-anion planes of the 4-layer thick Q slab (Fig. 10). This feature is analogous to that found in the layer structure of SnS (Wiedermeier and von Schnering 1978). It will be described in more detail below.

Coordination polyhedra

The averaged coordination octahedra in the H layer are very regular, 4 × 2.54 Å and 2 × 2.546 Å (Table 7). This can be compared with the Sn-S bond length in 2H-SnS_2 (Hazen and Finger 1978) equal to 2.564 Å. Data for Fe^{2+} from troilite and near-stoichiometric pyrrhotite (Keller-Besrest and Collin 1990a, 1990b) indicate the average of 2.492 Å (with a considerable range 2.356–2.721 Å) and 2.467/2.479 Å (range 2.423–2.524 Å), respectively. Values for Fe^{3+} are expected to be lower (2.42 Å, Shannon 1981). Thus, the average cation-anion bond length in the H layer points in the direction of Fe-for-Sn substitution without a real possibility to specify the valence of iron.

The average bond lengths in the outer cation position of the Q slab, Pb2 (Table 7), indicate preponderance of lead in this position. The vertex of the coordination pyramid of this cation, pointing into the interior of the Q slab, displays a bond distance

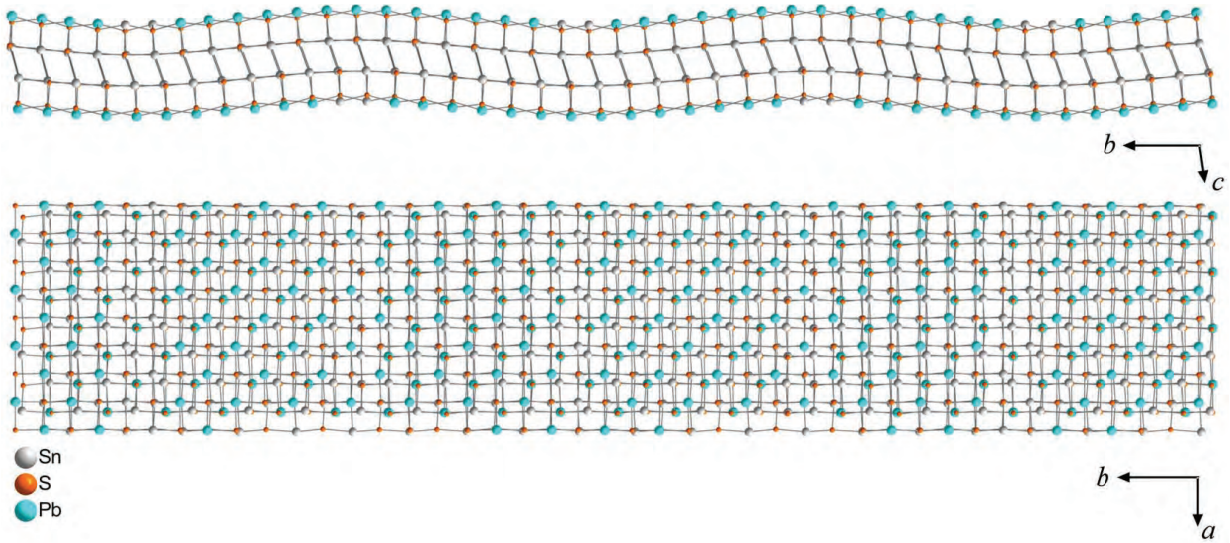

FIGURE 10. Structure of the pseudotetragonal Q slab in projection on (001) and on (100), respectively. The (001) projection suggests an explanation for the periodic shade variation in the HRTEM photographs of (001) franckeite flakes examined by Williams and Hyde (1988).

TABLE 7a. Selected interatomic distances (Å) in franckeite: H subsystem (ν = 1)

	Average	Min	Max
Sn1/Fe1-S1 (2×)	2.546(15)	2.518(14)	2.583(16)
Sn1/Fe1-S1^{i} (2×)	2.54(3)	2.50(3)	2.62(3)
Sn1/Fe1-S1^{ii} (2×)	2.54(3)	2.49(3)	2.61(3)

Notes: (i) x–1/2,y–1/2,z. (ii) x+1/2,y–1/2,z.

TABLE 7b. Selected interatomic distances (Å) in franckeite: Q subsystem (ν = 2), atom Pb2/Sn2

	Average	Min	Max
Pb2/Sn2-S2	2.95(2)	2.94(2)	2.993(19)
Pb2/Sn2-S2^{i}	2.97(2)	2.947(19)	2.99(2)
Pb2/Sn2-S2^{ii}	2.974(14)	2.819(14)	3.079(14)
Pb2/Sn2-S2^{iii}	3.010(15)	2.802(15)	3.163(15)
Pb2/Sn2-S3^{ii}	2.98(2)	2.95(2)	3.00(2)

Notes: (i) x+1,y,z. (ii) x+1/2,y–1/2,z. (iii) –x,–y+1,–z.

TABLE 7c. Selected interatomic distances (Å) in franckeite: H subsystem, atom Sn3/Pb3

	Average	Min	Max
Sn3/Pb3-S2	2.54(2)	2.46(2)	2.60(2)
Sn3/Pb3-S3^{i}	2.66(3)	2.61(3)	2.74(3)
Sn3/Pb3-S3	2.78(2)	2.73(2)	2.83(2)
Sn3/Pb3-S3^{ii}	3.12(2)	3.04(2)	3.17(2)
Sn3/Pb3-S3^{iii}	3.16(3)	3.09(3)	3.21(3)
Sn3/Pb3-S3^{iv}	3.48(2)	3.41(2)	3.56(2)

Notes: (i) x+1/2,y–1/2,z. (ii) x,y–1,z. (iii) x–1/2,y–1/2,z. (iv) –x+1/2,–y+5/2,–z–1.

equal to 2.98 Å, typical for Pb. The distances in the surface of the Q slab shows a pair of opposing distances 2.95 Å/3.01 Å accompanied by another pair of two nearly equal distances of 2.74 Å.

Configuration of the inner cation of the Q slab, "Pb3", is quite different and typical for a lone-electron pair element, such as Sn^{2+}/Sb^{3+}. The apical distance of 2.54 Å is accompanied by two additional short average "Sn"-S distances (2.66 and 2.78 Å) opposed by moderately long weak bonds (3.12 and 3.16 Å) in the inner plane of the Q slab. The three short distances are much shorter than the Pb-S bonds. Across the lone electron space of the Q slab, the nearest S atom is at an average distance of 3.48 Å. The observed distances can be compared with those of Sn^{2+} in SnS (Wiedemeier and von Schnering 1978): 2.627, 2 × 2.665, 2 × 3.290, and 3.388 Å and those of Sb^{3+} in Sb_2S_3 (Lundegaard et al. 2003): 2.450, 2 × 2.684, 2 × 2.850, and 3.363 Å for the inner site and 2.513, 2 × 2.541, 2 × 3.111, 3.164, and 3.637 Å for the marginal cation site of the "stibnite-like ribbon". The shortest distance agrees well with the presence of Sb in the mixed cation "Pb3" site, whereas the differences between the four distances in the base of square-pyramidal coordination are less pronounced than for Sn and for the marginal Sb in Sb_2S_3 but more extreme than those for the inner Sb site in stibnite.

This section shall be concluded by stressing the fact that each materialization of Sn1, Pb2, and Pb3 at a particular *t* value of the modulation wave is a result of all such materializations along the *u* values of the non-modulated misfit direction.

Geometric and compositional modulation

The Sn/Fe 1 position in the H layer, refined as 0.57(2) Sn and 0.43(2) Fe, is sinusoidally modulated in the *z* component with the amplitude of ~0.72 Å (Fig. 3), with negligible contributions from second- and third-order waves; the latter have an amplitude equal to 1/40 of the first-order sinusoid (Table 4). The positional modulation is connected with the oscillation of the occupational modulation about the 57% value (Table 5, Fig. 9). The inflection points are 11% richer in Sn than the regions of maximal curvature, which appear to concentrate Fe. Modest variations of interatomic distances (Fig. 11, Table 7) are correlated with these changes. The longest distances, up to 2.62 Å, occur at the crests and on the flanks of the sinusoid and are always coupled with the shortest distances, down to 2.49 Å. It is always only one pair of such values, presumably describing the opposing distances. Inflection points have the most equal distribution of bond distances (Fig. 11). The correlation of distance variations with increased Fe contents may be analogous to the above mentioned variations of Fe-S distances in FeS; the opposing trends in the changes of only two distances out of the six distances in the octahedral coordination appear to contradict a possible presence of Sb in these structure portions. Minor *y*-component of modulation of the cation position seen in Figure 3 and the elevated value of U_{11} (Table 6) might express these asymmetric coordinations.

The Q slab (Fig. 10) bears the bulk of modulation changes. Positional modulation is not complicated. The *z*-component, reaching an amplitude of ~0.74 Å for the Pb2 atom, is only very slightly modified by contributions of higher harmonics in a situation similar to that for the H layer (Fig. 4, Table 4). The considerable *y* component, with a phase shift against the *z* component, is much larger for the outer Pb2 position (Fig. 4) than for the inner Pb3 position (Fig. 6). It has already been explained above as a result of sinusoidal bending of a semirigid 4-layer thick Q slab. The same *z*- and *y*-modulation is observed for S2 and S3. The *y*-component of these two sites appears to express additional modulation (Figs. 5 and 7) that apparently is produced by a distribution of unequally long cation-anion distances in the (001) cation-anion sheets. The variations of the latter are also expressed by augmented values of U_{11} and U_{22} of S3 (Table 6), whereas cation substitutions in the Pb3 site might cause elevated value of U_{33} for S2.

The cation occupation scheme of the Q slab is complex. In the convex region between two inflection points, an occupational plateau for Pb2 site (Fig. 8) is situated with ~0.8 Pb and ~0.2

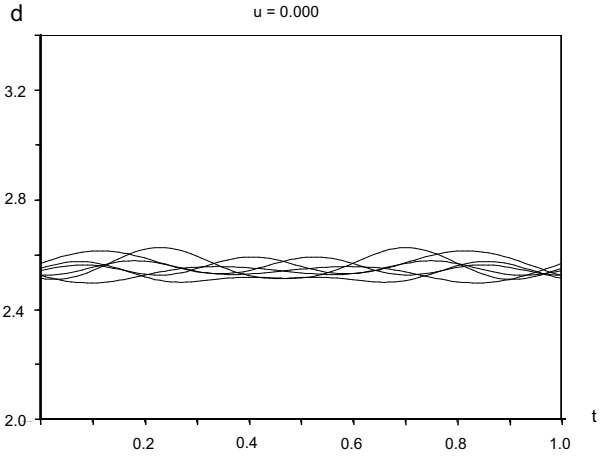

FIGURE 11. Modulation of the six Sn1–S1 distances in the H layer along the parameter *t*.

(Sn/Sb). The slightly wavy character of this region might be an artificial cut-off feature. The concave region, however, displays a pronounced dip in the average atomic number, reaching 0.58 Sn/Sb, i.e., only 0.42 Pb. This is in agreement with HRTEM observations of Wang (1989) and Wang and Kuo (1991) and various similar observations made for cylindrite that were summarized by Makovicky et al. (2008). The strict localization of this substitution to the concave part of the wave appears logical but the flatness of the occupation ratio of convex portions and the Pb-rich character of the inflection region is remarkable. The changes in the occupation of the Pb2 site are correlated with those in the Pb3 site. The average occupancy of the Pb3 site (Fig. 8, Table 4) was refined as 0.27(2) Pb and 0.73(2) Sn/Sb. In the concave region, it reaches 0.92 Sn/Sb and only 0.08 Pb, whereas in the rest of the layer it forms a plateau at about 0.70 Sn/Sb.

The intralayer Pb2-S distances (Fig. 12) vary modestly with these changes. Three distances stay just below 3.0 Å, whereas two distances drop to about 2.8 Å for the concave region and increase in the center of the plateau; one of them reaches almost 3.2 Å. This is the distance to S2 at –x,–y+1,–z and it swings from the absolute minimum to the maximum. Variation of the Pb2-S3 distance, i.e., to the vertex of the coordination pyramid of this cation, is modest as well (Table 7). The cation-anion distances of the inner cation "Pb3" follow a typical 3+2+1 pattern of distances for a lone electron pair element (Fig. 13, Table 7). A slight decrease of two short distances is observed in the concave Sn/Sb-enriched region, whereas smaller differences between bond lengths exist in the regions with a higher Pb content. The longest Sn/Sb/Pb-S distance, across the central lone electron pair micelle, decreases slightly in the latter regions but its distribution is displaced along **b**, apparently because of the atomic shifts across the space of the micelle.

Interlayer configurations

For the cylindrite structure type, Makovicky et al. (2008) stated that the transversal modulation of the structure is the way of achieving commensurability of large portions of interlayer space by "enveloping", in a commensurate manner, a convex surface of the Q slab that displays shorter periodicity by the concave H layer with longer periodicity. In this way, the 2D-misfit is reduced to 1D-misfit that is orientated along the non-modulated direction, which serves as cylinder tangent. In the concave portions of the Q surface, problems are solved by insertion of short intervals with a different cation configuration, with interlayer anion-cation connections spread in a fan-like manner.

The present investigation shows that the same principle is valid for franckeite (Fig. 14). With the high contents of Pb in the Q slab, the dimensions of the Q cell are larger than they were for the examined cylindrite, whereas those of the H cell are not affected. Thus, for curvatures allowed by the crystal chemistry of the Q slab, the regions of commensurability on a curved surface are considerably longer, about 5 $\mathbf{b}_Q$ long, than the lengths of only 3 $\mathbf{b}_Q$ that were observed for the Sn-Se isotype of cylindrite. On these convexly curved portions, the [100] atom rows of the Q surface fit symmetrically into "grooves" between two adjacent [100] sulfur rows on the surface of the H layer (Fig. 14). In the concave portions of the Q slab, populated by Sn/Sb/(Pb), two to four cations lie directly or almost directly opposite the S rows of the convex H layer. Transitional interval between these two modes of interlayer match is narrow.

Similar to the layer misfit structures of the generalized cylindrite structure type, levyclaudite (Evain et al. 2006) and the Sn-Se cylindrite (Makovicky et al. 2008), the interlayer distances represent a complex picture that is a 2D-function of the *t* and *u* modulation parameters (Figs. 15a–15c). Usually three (or less) cation-anion distances ≤4 Å are observed at any combination of *u* and *t* parameters. Three characteristic situations were selected from the spectrum of distances; the rest are transitional cases between them. The shortest observed interlayer distance of 2.652(17) Å to S1 can be materialized as the only well-documented case of interlayer bonding at, and only at, the *u* value equal to 0.230 combined with a *t* value corresponding to the most concave position(s) of Pb2 (Fig. 15a). These are the sites that exhibit the Z values corresponding to predominant Sn/Sb (Fig. 15a). For *u* equal to 0.470, this particular *t* position shows

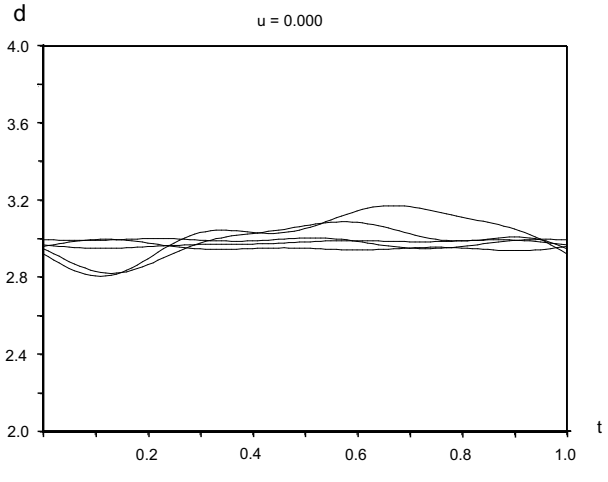

Figure 12. Modulation of the intra-slab cation–anion distances for the Pb2 position from the Q slab. The abscissa is identical with that in Figure 4.

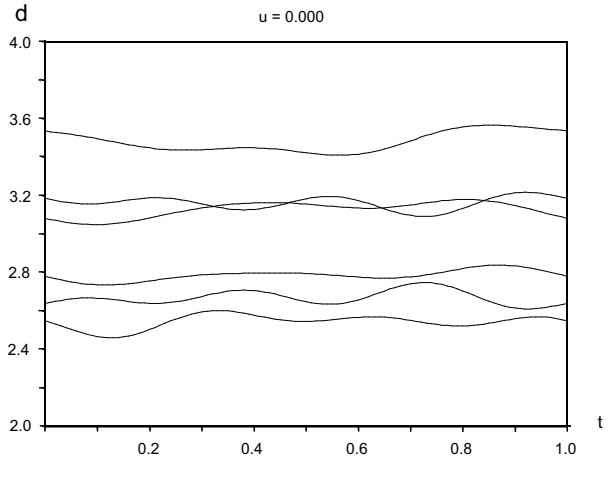

Figure 13. Six significant cation-anion distances for the "Pb3" position in the interior of the Q slab. A pattern typical for a lone-electron-pair cation is observed. The longest distance is that across the lone-electron-pair micelle in the median plane of the Q slab.

a cation-anion distance equal to 2.8 Å, whereas for other *t* values along the modulation wave a uniform distance of about 2.9 Å is demonstrated (Fig. 15b). Then the distances increase until a situation with all interlayer cation-anion distances between 3.0 and 3.2 Å is reached at $u = 0.720$ (Fig. 15c).

Definition of archetype for the Q layer

The outer planes of the Q slab (four atomic layers thick) consist of fairly regular coordination squares of Pb2; these are present in the straight, convex, or concave regions. In the latter regions, the majority cation Pb is replaced by a cation with a lower Z value and somewhat shorter cation-anion distances. The specificity of the Q slab is caused, however, by the configuration of the two inner atomic planes that contain the "Pb3" site. According to the results of the structure determination, this site is mainly occupied by Sn and/or Sb. Presumably it concentrates Sb because of the similarity of this configuration to those observed in many Pb-Sb sulfosalts. Each of these planes forms a tightly bonded layer pair with the adjacent Pb2-S2 plane on the outside of the Q slab. The space between the "Pb3"-S3 atomic

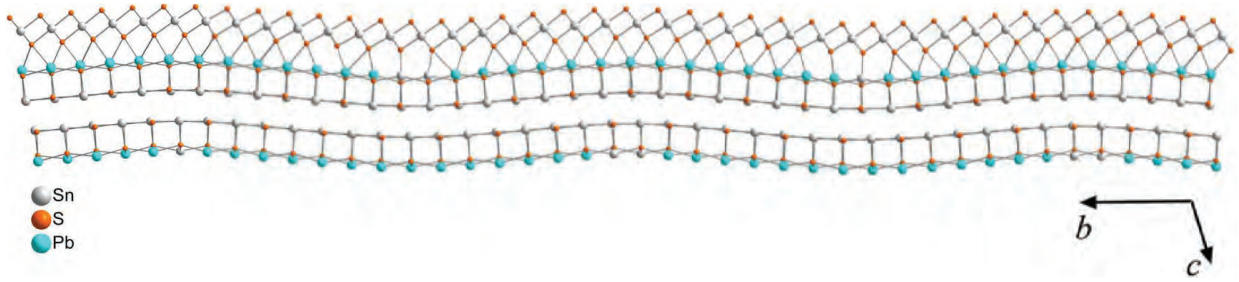

FIGURE 14. A detail of a Q–H pair of planes illustrating the pattern of interlayer distances, which alternately assume two distinct configurations, seen in the concave and the convex portions of the Q surface, respectively. Details are discussed in the text.

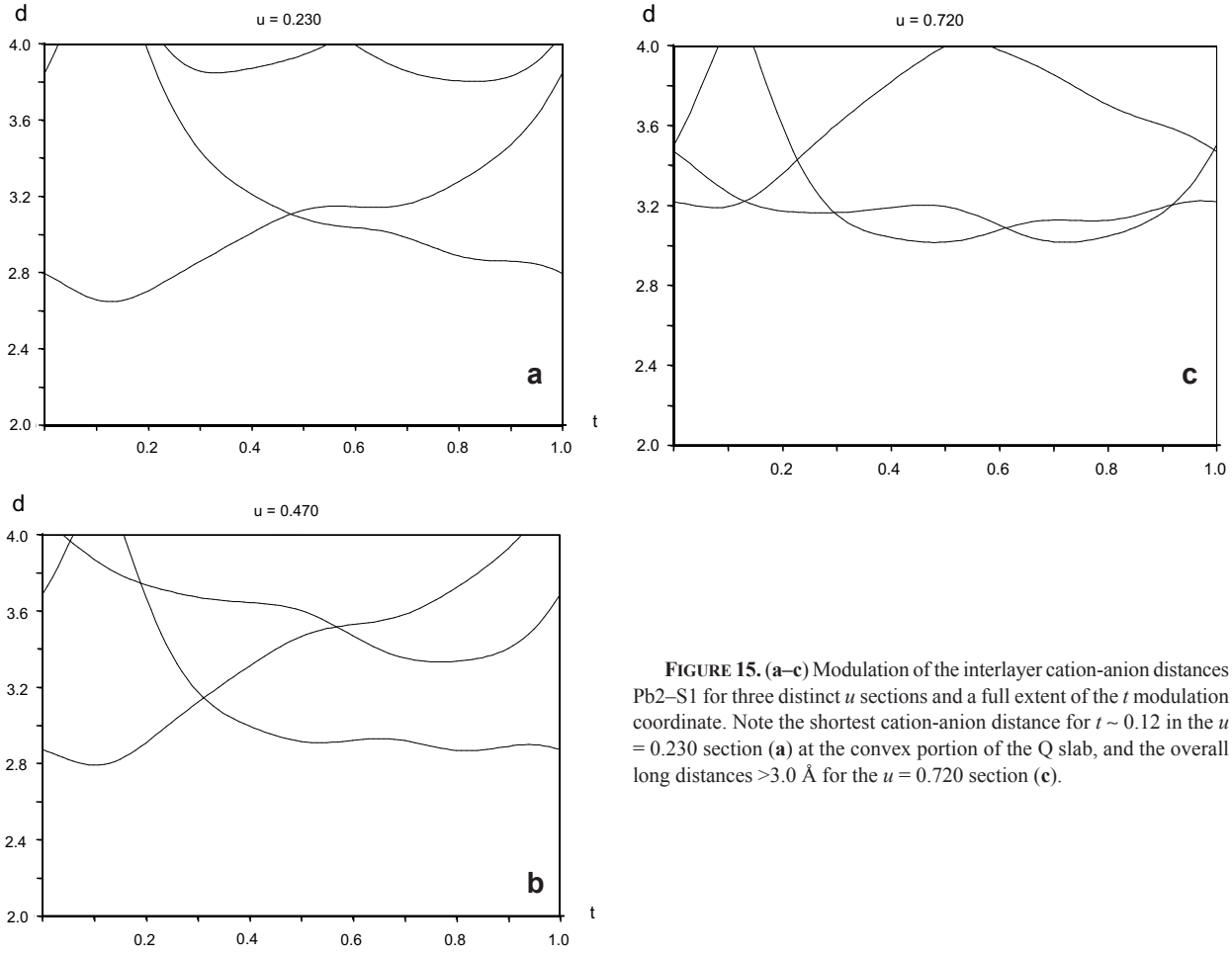

FIGURE 15. (**a–c**) Modulation of the interlayer cation-anion distances Pb2–S1 for three distinct *u* sections and a full extent of the *t* modulation coordinate. Note the shortest cation-anion distance for $t \sim 0.12$ in the $u = 0.230$ section (**a**) at the convex portion of the Q slab, and the overall long distances >3.0 Å for the $u = 0.720$ section (**c**).

planes accommodates the non-bonding electron pairs of "Pb3", i.e., mainly of Sb^{3+} and Sn^{2+}. In accordance with this, "Pb3" has two short, strong bonds to S3 and two longer, weaker bonds to opposing S3 in its own Pb3-S3 plane, accompanied by a long Pb3-S3 distance to the S3 atom in the adjacent Pb3-S3 plane, across the core of the central lone electron pair micelle (Fig. 10).

The short Pb3-S3 bonds form chains parallel to [1$\bar{1}$0], which are spaced *d*(110) apart (Figs. 16 and 17). Although the chains of short bonds are parallel, short bond pairs of "Pb3" in the two planes surrounding the same central micelle space are oriented opposite to one another. The resulting configuration of two double-layers copies the one observed in SnS at ambient conditions (Wiedermeier and von Schnering 1978). The pair of double-layers corresponds only to one half of the double-layer sequence in SnS. Therefore it cannot be described using a full 3D cell of SnS, only an intralayer mesh taken from the latter, to which the third, non-periodic direction is perpendicular. The primitive square mesh has the **b** direction (perpendicular to the bond-chains) parallel to [011], the **c** direction, parallel to the chains along [1$\bar{1}$0], and the layer-stacking parameter **a** across the Q slab. The consistent orientation of the SnS like motif in an untwinned structure and its weak expression on the surface of the Q slab are noteworthy.

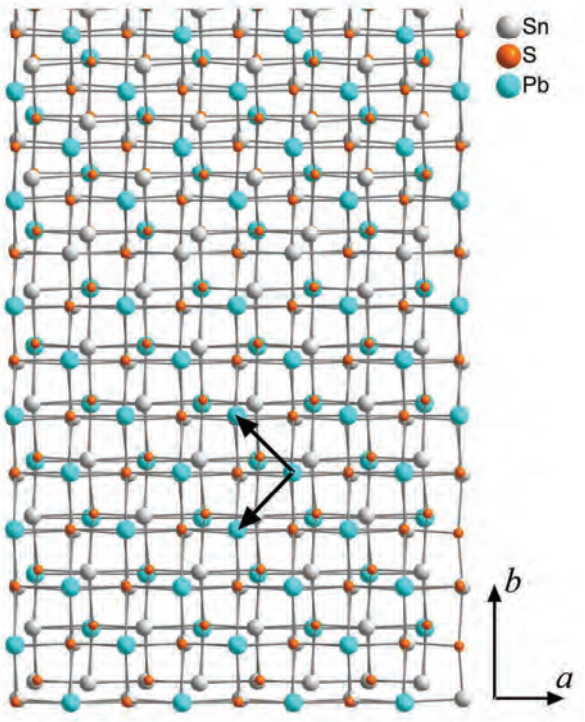

FIGURE 16. A detail of the structure of the Q slab in a perpendicular projection. Pb2 atoms form the top and the bottom planes, respectively [blue except for the concave region in the upper part of the figure, which contains a row of silver-colored (Sn,Sb)-rich sites]. There are two planes of "Pb3" sites, predominantly (Sn,Sb) (silver-colored). The Q slab, consisting of two strongly bonded double-layers and a lone electron micelle between them, corresponds to a cut-out from the crystal structure of SnS. The axes of the SnS-like submesh, oriented diagonally to the present axes, are shown in the central parts.

Layer chemistry

The structural formula of franckeite is a function of interlayer match. This will be approximated by a simple, close match of 16 Q cells with 15 H cells [both *C*-centered] (i.e., 93.78 Å) in the **b** direction, and a selection of the best "near-coincidence interval" between the two components in the **a** direction: 6 Q cells with 9.5 H cells (giving the length of 34.83 Å). Each Q cell contains $Me_2S_2 \times 4 = Me_8S_8$. The column of 16 Q cells contains $Me_{128}S_{128}$. This matches with H cells: the contents of each H cell (containing 2 coordination octahedra) are Me_2S_4, and the column is $Me_2S_4 \times 15 = Me_{30}S_{60}$. The $6 \times$ [Q component] gives $Me_{768}S_{768}$, matching with $9.5 \times$ [H component] = $Me_{285}S_{570}$. The resulting formula is $Me^{Q}_{768}Me^{H}_{285}S^{Q}_{768}S^{H}_{570}$, i.e., $Me_{1053}S_{1338}$.

When the results of microprobe analyses are recalculated to the number of cations contained in this large coincidence mesh (standard deviations in parentheses are in terms of the last digit) we obtain

$Pb_{501.36(268)}Ag_{14.64(73)}Cu_{0.73(49)}Fe_{96.42(195)}Sn_{227.98(171)}Sb_{211.87(293)}S_{1388.13(561)}$.

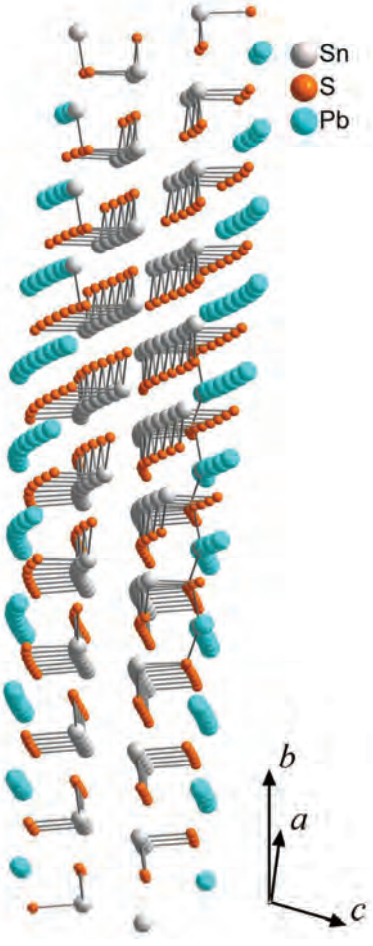

FIGURE 17. The same portion of the Q slab as in Figure 16, projected onto the (1$\bar{1}$0) plane (the symmetry plane of the SnS-like submotif in Fig. 16). Only the short, strong bonds of the lone-electron-pair cations Sn^{2+} and Sb^{3+} have been drawn. Convolution of the SnS-like pattern of short bonds with layer modulation is illustrated.

When Pb and all of Sb, as well as Ag and traces of Cu are assigned to Q slabs, they occupy 728.60 sites, leaving 39.40 sites for Sn^{2+}. This leaves 188.58 Sn^{4+} and 96.42 Fe, resulting in the 285 Me^{H} atoms as expected. We do not believe in large cation vacancies in a structure composed of fairly thin layers (it would collapse and reform) and therefore we base our calculations on the sum of cation sites as observed in the structure determination and not on the analytical sulfur content obtained for this mineral with five distinct cation species and a very heavy lead presence. Thus, the number of S atoms in agreement with the structure model is assumed.

Valence calculations based on these results, counting with the presence of both Sn^{2+} and Sn^{4+} and with Fe^{2+} are +196.5 charge units for the above-defined coincidence mesh in the Q slab and –192.8 for the same mesh in the H layer. The difference lies below the accuracy of the microprobe analysis and of the geometrical approximation used. This calculation proves the interdependence of the Q and H layers that justifies their regular alternation. At the same time it indicates that iron in franckeite is in a divalent state.

The model chemical ratio based on microprobe analyses is 501.36 Pb:39.40 Sn^{2+}, i.e., 501.36/540.76, i.e., 92.7% of the ideal Sn^{2+}-free plumbian-franckeite end-member ("end-member potosiite"). This agrees with the observed Q:H match, which is very far from the 12:11 match that was found by Li et al. (1988) for pure Sn cylindrite and might apply also to the Pb-free franckeite.

At the current stage of research, derivation of a general chemical formula for franckeite is hampered by the absence of reliable data on the Q:H matches observed for different members of the Sn^{2+}-Pb solid-solution series. The match ratios along the **b** direction are known at least schematically, from 12:11 to 16:15 as quoted above, but those along the **a** direction remain virtually unexplored. Use of powder data is hampered by overlaps of critical *d* values related to the intralayer dimensions with those related to the layer stacking period (e.g., 3 × 5.8 Å = 17.4 Å).

A comparison of chemical composition estimated from the electron microprobe analysis with that obtained from the structure refinement shows that the modulated refinement with sulfur sites fixed at full occupancy values underestimates somewhat the Z values of cations in the Q and H layers. The overall Z_{Me}/Z_S ratio from the chemical analysis is 3.108, whereas the same ratio obtained from the refinement is 2.907. For the H layer, the same ratio is 1.309 vs. the structural ratio 1.239, and for the Q slab it is 4.443 vs. 4.143, i.e., approximately the same for both components. This has bearing on the Fe/Sn and Pb/(Sn+Sb) ratios estimated by the two approaches.

Layer stacking: the a × c plane

In the **b** × **c** plane, the stacking directions of both components coincide, resulting in the α angle equal to ~95°. In the **a** × **c** plane, however, these directions differ, and each set of layers/slabs follows its own stacking direction (Fig. 18). Unlike the situation in synthetic Sn-Se cylindrite isotype, the H component has a large β value equal to 95.45° and the Q component has β equal to 88.71°, i.e., close to 90.6°, which was displayed by the H component in cylindrite (Makovicky et al. 2008). Significantly, Δβ in franckeite, equal to 7.74°, is nearly identical to Δβ in Sn-Se cylindrite, equal to 7.45°, suggesting that similar rules govern stacking of H:Q sequences in both compounds. Two apparent stackings, one with β_H value approximately 90° and another one with β_Q value equal to ~98°, have the **c** stacking vectors doubled because they form a part of a centered **a** × **c** mesh. The Δβ difference defines a relative shift of the H component against the Q stacking direction, that is equal to 3.5 a_H for a H layer situated after six intervening Q slabs.

The divergence of the stacking vectors of the H and Q layer sets has two components, respectively, generated by (1) the SnS-like configuration in the interior of the Q slabs, offsetting the distal surface of the slab against the proximal one (Fig. 18), and (2) the Q–H–Q interlayer configuration. The latter approximates locally the situation seen in Sn-Se cylindrite although somewhat different a_H/a_Q ratios have to be considered.

A net of approximate interlayer matches can be drawn graphically in Figure 18, in which an arbitrarily selected projected H/Q match situation has been chosen and mapped out. It is related to the H cell as follows:

$$\mathbf{a}_{net} = 8\mathbf{a}_H \sim 5\mathbf{a}_Q \text{ and } \mathbf{c}_{net} = \mathbf{c}_H - \mathbf{a}_H$$

Actually, for the H component the match repeats already after four $\mathbf{a}_H$, but the match takes place with the centering points of the Q cell. The degree of approximation in this concept can be seen from the comparison of $8a_H$ (29.32 Å) with the "matching" $5a_Q$ (29.01 Å). This quasi-periodicity of large-scale matching situations is strengthened further by local situations: in Figure 18, we can observe that any type of local interlayer Q-H match is immediately paralleled by an opposite type of interlayer H-Q configuration on the other side of the H layer. This can also be observed for Sn-Se cylindrite, in Figure 6 of Makovicky et al. (2008).

We cannot escape a suggestion that the morphological instability of franckeite, and even more that of cylindrite (Makovicky et al. 2008) in the **b** direction, described as a consequence of unmodulated incommensurability of the two layer sets, H and Q, in this direction, is strengthened by a tendency to restore again and again the observed and illustrated interlayer match. The 8 $\mathbf{a}_H \sim 5\ \mathbf{a}_Q$ mismatch described above accumulates a misfit of about 1 Å for every 100 Å along the **a** direction and of more than one full a_H parameter for every 400 Å. A correction of the rising misfit may take place by curving the layer pair with the **b** vector as a tangent and the H layer on the outside (i.e., a Q→H interface). In a layer stack this will produce a series of dislocations, especially on an H→Q interface. It should be noted however that, as observed by Makovicky (1976) and Makovicky and Hyde (1981), stacking of H and Q layers in natural cylindrical cylindrite follows principles different from those observed in a flat aggregate.

Layer stacking: the b × c plane

The transversal modulation of both layer types is close to sinusoidal; slight departures from this geometry observed for the Q component have already been mentioned. They are in direct connection with the patterns of occupancy of the outer, Pb2, and the inner, "Pb3", cation sites in the Q slab (Fig. 8). Instead of si-

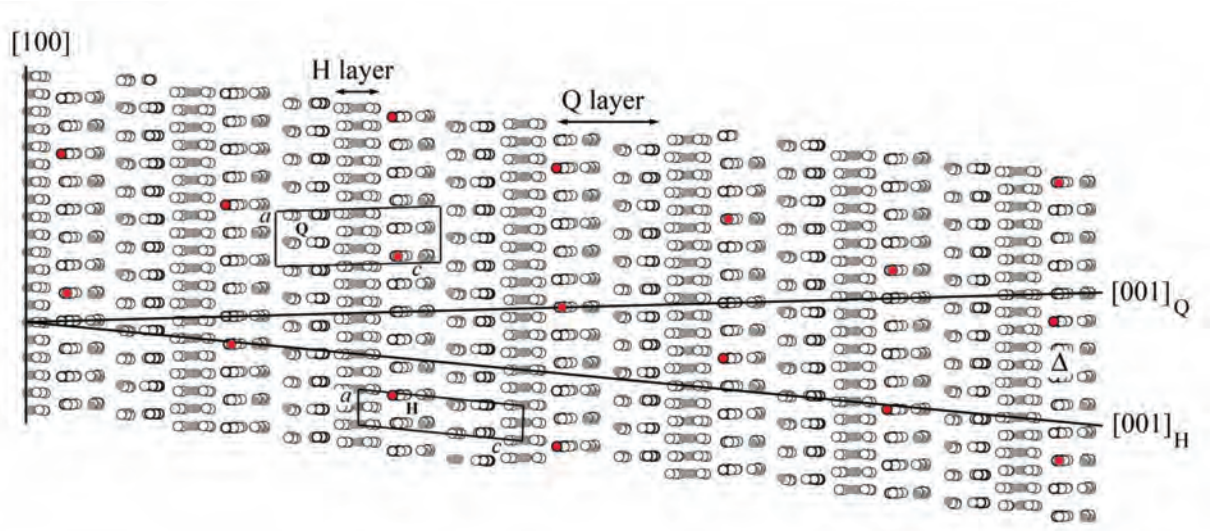

FIGURE 18. Projection of an (010) slice of the crystal structure of franckeite along [010] ("the **a** × **c** projection") showing alternation of the H and Q slabs. Diverging *c* periodicities and the cells of the two components are illustrated. Red marks denote approximate repetition of a pre-selected interlayer match mode of atomic rows [010] of the two components through the layer pile. Detailed discussion of all relationships is given in the text.

nusoidal Pb:(Sn,Sb) occupational modulation, these sites display a sharp concentration of (Sn, Sb) in the concave intervals of the transversally modulated slab and a fairly uniform, Pb-enriched situation between these sharply delineated intervals, giving rise to a slightly non-sinusoidal shape of the layer.

The layer-stacking direction **c** and the α angle of franckeite (Fig. 19) are determined by a combination of (1) interlayer Q-H-Q match and (2) a [010] component of the SnS like displacement in the lone electron pair micelle of the Q slab in the **b** × **c** plane. The former corresponds in principle and configuration to the situation observed in Sn-Se cylindrite, whereas the latter, together with the additional thickness of the Q slab, modifies the α angle. An additional factor is the difference in the β_H angle observed in cylindrite and in franckeite, respectively (discussed above), which causes different *b*-shifts of the H layers in these two structures when studying an individual **b** × **c** plane. These three principles combine and result in the larger α value for franckeite.

The oblique stacking of H and Q layers is in contradiction to the requirements of transversal modulation that, to satisfy the coordination and configuration requirements of cations and anions in the layers and *on their interfaces* must have the wave normal parallel to the **b** vector, i.e., situated in the (001) plane. Wave fronts are then perpendicular to the layers and deviate from the **c** stacking vectors (Fig. 19). No [010] shifts of consecutive layers by integral number of *b* parameters are observed that would resolve this situation, and instead of it, the consecutive layers "slide smoothly" over the modulation by small increments, similar to the situation observed in cylindrite (Makovicky et al. 2008).

Absence of reflections indicating superperiods in the **c** direction indicates that all layers of each subset (i.e., all Q and all H layers, respectively) in the structure are equivalent and the **c** period observed is a true period. This can be achieved only if every geometric relationship between the cell repetition and the modulation wave observed for the *n*th layer along **c** can be found also in the first, and any consecutive *m*th layer ($m \neq n$) at a certain point along **b.** The geometrical condition implied is that the [010] period defined by the match of *m*Q and *n*H cells differs by a small increment Δ*b* from that defined by the modulation vector. As described above, Δ*b* is 0.24 Å in the present case and it was 0.30 Å for the other franckeite sample. With the large periodicities involved, the estimates of these Δ values are subject to a degree of experimental error.

Twinning of franckeite

The universally observed twinning of franckeite, with the **b** direction as a twin axis, and with an inevitable glide component equal to ½ *t* added to accommodate modulation, indicates that the Q-H-Q match pattern described in the previous paragraphs is maintained on twinning, ensuring the stability of the twinned structure. Twinning rotates both the H and Q layers and thus results in two most significant changes: the orientation of the H layers and the resulting orientation of the α angle is reversed and the orientation of the short-bond chains in the interior of the Q slabs reverses from the original [1$\bar{1}$0] direction to the [110] direction when indexed in terms of the original axial system. These two directions are perpendicular to one another and feasibility of this twinning confirms that the SnS-like unit mesh of franckeite Q slabs is practically a square mesh.

CONCLUDING REMARKS

Similar to its close relative, cylindrite, franckeite is not a single mineral with a Sn^{2+}-Pb solid solution active in a fundamentally unchanged crystal structure as, e.g., is a tin-containing jamesonite from Dachang, China, or from Bolivian deposits. Its two-dimensionally non-commensurate misfit-layer character (Makovicky and Hyde 1992) means that changes in chemistry alter the interlayer match both in the non-modulated **a** and the modulated **b** direction and although the governing structural principles remain preserved, the actual geometry of the structure changes. The special type of

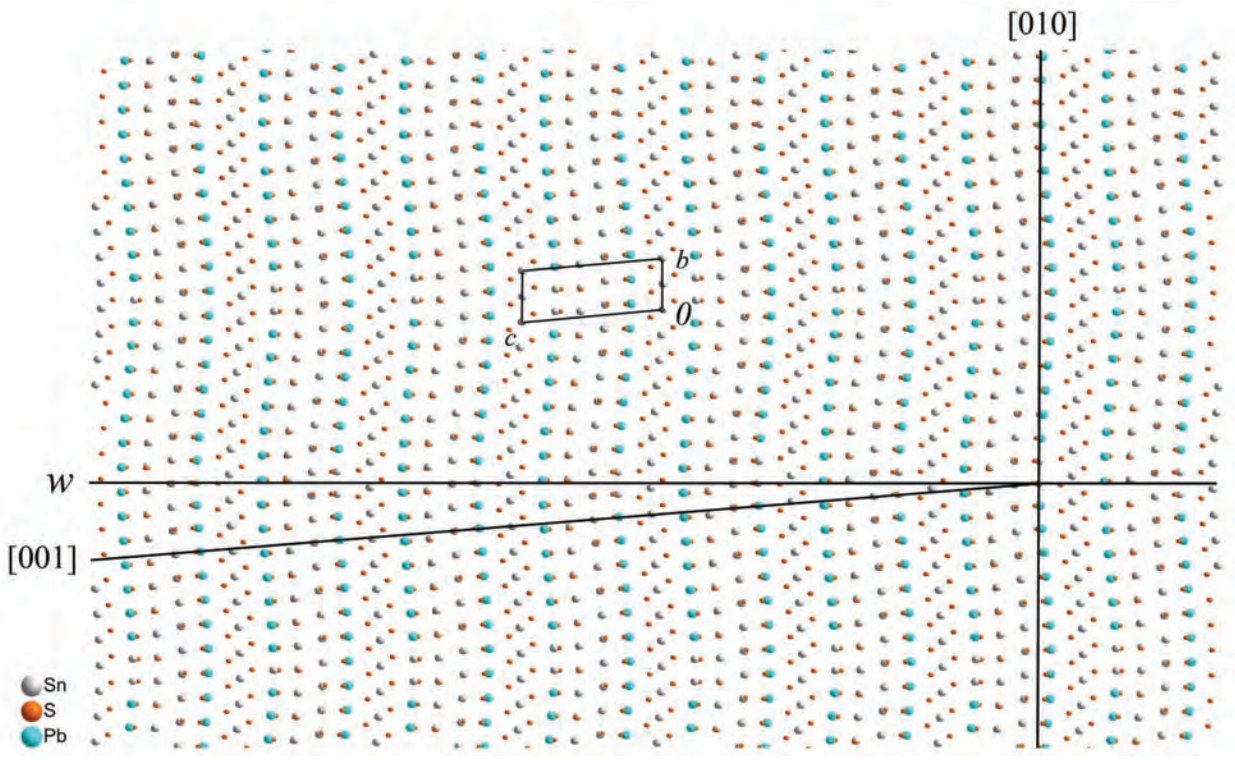

FIGURE 19. Projection of the crystal structure of franckeite along [100] ("the **b** × **c** projection") showing alternation of modulated H and Q slabs. Projection of the H and Q cells (identical in projection), a (projected) propagation vector of the underlying layer structure and the wavefront of modulation (*w*) are indicated. Detailed discussion of all relationships seen in this projection is given in the text.

local commensurability on curved surfaces in the general **b** direction of the transversally modulated structure dictates step-like changes in the interlayer match along this direction concurrent with the changes in chemistry, whereas the changes along the non-modulated **a** direction do not have this limitation.

Therefore, franckeite is a *variable-fit series* of very close phases with the same structural principle but a quantitatively different interlayer matches and modulation periodicities. Further examples of series of this kind can be found in Makovicky and Hyde (1981, 1992). Phases of a variable-fit series are chemically and structurally so close that they should bear a single mineral-species name, with the interlayer match scheme specified, e.g., franckeite 15.5Q:14.5H in the present case.

The existence of the cylindrite-franckeite family depends critically on the radius ratios of the cations involved in the two layer types, especially on a combination of (Pb^{2+}, Sn^{2+}) in the pseudotetragonal layers with Sn^{4+} in the pseudohexagonal layers. As discussed in detail by Makovicky and Hyde (1992), their replacement by a Pb^{2+}-Bi^{3+} combination in both layer types leads to misfit layer structures of a very different type, typified by cannizzarite.

ACKNOWLEDGMENTS

The work has been supported by the grant no. 272-08-0227 of the National Research Council for Nature and Universe of Denmark, by the Praemium Academiae fund of the Czech Academy of Sciences, by the institutional research plan no. AVOZ10100521 of the Institute of Physics of this Academy, and by the Christian Doppler Foundation of Austria. Inspiring reviews by Yves Moëlo and M. Pasero as well as the assistance of the associate editor F. Colombo are gratefully acknowledged.

REFERENCES CITED

Ahlfeld, F. and Moritz, H. (1933) Beitrag zur Kenntnis der Sulfostannate Boliviens. Neues Jahrbuch für Mineralogie, Beilage–Band, 66, 179–212.

Amthauer, G. (1986) Crystal chemistry and valencies of iron, antimony, and tin in franckeites. Neues Jahrbuch für Mineralogie, Abhandlungen, 153, 272–278.

Bernhardt, H.-J. (1984) The composition of natural franckeites. Neues Jahrbuch für Mineralogie, Abhandlungen, 150, 41–45.

Bonshtedt-Kupletskaya, E.M. and Chukhrov, F.V., Eds. (1960) Mineraly—spravochnik, vol. 1, 616 p. Academy of Sciences USSR Publishing House, Moscow.

Coulon, M., Heitz, F., and Le Bihan, M.T. (1961) Contribution à l'étude structurale d'un sulfure de plomb, d'antimoine et d'étain: la franckéite. Bulletin de la Societé française de Minéralogie et Cristallographie, 84, 350–353.

Evain, M., Petříček, V., Moëlo,Y., and Maurel, C. (2006) First (3+2)-dimensional superspace approach to the structure of lévyclaudite–(Sb), a member of the cylindrite-type minerals. Acta Crystallographica, B62, 775–789.

Hazen, R.M. and Finger, L.W. (1978) The crystal structures and compressibilities of layer minerals at high pressure. I. SnS_2, berndtite. American Mineralogist, 63, 289–292.

Henriksen, R.B., Makovicky, E., Stipp, S.L.S., Nissen, C., and Eggleston, C.M. (2002) Atomic scale observations of franckeite surface morphology. American Mineralogist, 87, 1273–1278.

Huang, M., Wu, G., Chen, Y., and Tang, Sh. (1986) Mineralogical study of the franckeite from the Dachang cassiterite-sulphide polymetallic ore field, Guangxi. Acta Geologica Sinica, 2, 164–175 (in Chinese).

Hunger, H.-J., Wolf, M., Bewilogua, K., and Mehner, H. (1986) Crystallographic investigations on minerals of the cylindrite—franckeite group. Proceedings of the XIIth Conference on Applied Crystallography, Cieszyn, August, 10–14.

Janssen, T., Janner, A., Looijenga-Loos, A., and de Wolff, P.M. (1999) Incommensurate and commensurate modulated structures. International Tables for Crystallography, vol. C, 899-937. IUCr-Kluwer Academic Publishers, Dodrecht.

Keller-Besrest, F. and Collin, G. (1990a) Structural aspects of the alpha transition in stoichiometric FeS: identification of the high-temperature phase. Journal of Solid State Chemistry, 84, 194–210.

——— (1990b) Structural aspects of the alpha transition in off-stoichiometric $Fe_{1-x}S$ crystals. Journal of Solid State Chemistry, 84, 271–275.

Kissin, S.A. and Owens, D.R. (1986) The properties and modulated structure of

potosiite from the Cassiar district, British Columbia. Canadian Mineralogist, 24, 45–50.
Korekawa, M. (1968) Theorie der Satellitenreflexe. Habilitationsschrift, Universität München.
Li, J. (1984) Franckeite syntheses and heating experiments. Neues Jahrbuch für Mineralogie, Abhandlungen, 150, 45–50.
——— (1989) Synthetic Ag-bearing franckeite and its mineralogical significance. Neues Jahrbuch für Mineralogie, Abhandlungen, 160, 36–37.
——— (1990) Die polymetallischen Kassiterit–Sulfiderz-Paragenesen von Dachang/China unter besonderer Berücksichtigung der Sulfosalze. Ph.D. thesis, University of Heidelberg.
Li, J., Huang, J., Zhou, K., and Zhang, G. (1988) An experimental study on three quaternary phases in the Fe-Sn-Sb-S system: Pb-free franckeite, Pb-free cylindrite and (Fe,Sb)-ottemannite s.s. Acta Geologica Sinica, 1, 393–405.
Lundegaard, L.F., Miletich, R., Balić-Žunić, T., and Makovicky, E. (2003) Equation of state and crystal structure of Sb_2S_3 between 0 and 10 GPa. Physics and Chemistry of Minerals, 30, 463–468.
Ma, Z, Zhao, X., and Shi, N. (1997) STM study of franckeite surface. Acta Petrologica et Mineralogica, 16, 237–243 (in Chinese).
Makovicky, E. (1970) Cylindrite—Crystallography, Crystal Structure and Chemical Composition. Ph.D. thesis, McGill University, Montreal.
——— (1974) Mineralogical data on cylindrite and incaite. Neues Jahrbuch für Mineralogie, Monatshefte, 235–256.
——— (1976) Crystallography of cylindrite. Part. I. Crystal lattices of cylindrite and incaite. Neues Jahrbuch für Mineralogie, Abhandlungen, 126, 304–326.
——— (1997) Modular crystal chemistry of sulphosalts and other complex sulphides. In S. Merlino, Ed., Modular Aspects of Minerals, 1, p. 237–274. European Mineralogical Union (EMU) Notes in Mineralogy, Eötvös University Press, Budapest.
——— (2005) Modular aspects of inorganic and mineral structures. Acta Crystallographica, A61, C129–C130.
Makovicky, E. and Hyde, B.G. (1981) Non-commensurate (misfit) layer structures. Structure and Bonding, 46, 101–176.
——— (1992) Incommensurate, two-layer structures with complex crystal chemistry: minerals and related synthetics. Materials Science Forum, 100/101, 1–100.
Makovicky, E. and Mumme, W.G. (1983) The crystal structure of ramdohrite, $Pb_6Sb_{11}Ag_3S_{24}$, and its implications for the andorite group and zinckenite. Neues Jahrbuch Mineral, Abhandlungen, 147, 58–79.
Makovicky, E., Petříček, V., Dušek, M., and Topa, D. (2008) Crystal structure of a synthetic tin-selenium representative of the cylindrite structure type. American Mineralogist, 93, 1787–1798.
Manapov, R.A. and Pen'kov, I.N. (1976) Nuclear gamma resonance of Sn^{119} and Fe^{57} in franckeite and cylindrite. Doklady Akademii Nauk SSSR, 228, 103–105 (English translation).
Moh, G. and Li, J. (1986) Paragenesis and genesis of the tin-bearing sulfide ores in Dachang/China. Neues Jahrbuch für Mineralogie, Abhandlungen, 153, 267–272.
Mozgova, N.N. (1983) On non-stoichiometry of franckeites-cylindrites and their crystal-chemical properties. Izvestiya Akademii Nauk SSSR, Geological Series, 9, 107–123.
Mozgova, N.N., Borodayev, Yu, S., and Sveshnikova, O.L. (1975) New-data on franckeite and cylindrite. Doklady Akademii Nauk SSSR, 220, 191–194 (in Russian).
Mozgova, N.N., Organova, N.I., and Gorshkov, A.I. (1976) On structural identity of incaite and franckeite. Doklady Akademii Nauk SSSR, 228, 705–708.
Mozgova, N.N., Borodayev, Yu.S., and Organova, N.I. (1977) Polyphase character of franckeite and cylindrite aggregates In F.V. Chukhrov and N.V. Petrovskaya, Eds., Inhomogeneity of Minerals and Fine-Grained Mineral Mixtures. Nauka, Moscow (in Russian).
Nekrasov, I. Ya., Bortnikov, N.S., and Tsepin, L.I. (1975) Synthesis and phase relations of sulfostannates of the Pb-Sn-Sb-S system under hydrothermal conditions. Doklady Akademii Nauk SSSR, 223, 707–710.
Organova, N.I., Dmitrik, A.L., and Laputina, I.P. (1980) On the structure of franckeite. Geochemistry and Mineralogy: Contributions of Soviet Geologists at the XXVI Congress IGC, Moscow, p. 101–108 (in Russian).
Oxford Diffraction (2009) CrysAlis CCD, CrysAlisRED and CrysAlis PRO. Oxford Diffraction, Oxforshire, England.
Paar, W.H., Moëlo, Y., Mozgova, N.N., Organova, N.I., Stanley, C.J., Roberts, A.C., Culetto, F.J., Effenberger, H.S., Topa, D., Putz, H., Sureda, R.J., and de Brodtkorb, M.K. (2008) Coiraite, $(Pb, Sn^{2+})_{12.5}As_5Fe^{2+}Sn^{4+}{}_5S_{28}$: a franckeite-type new mineral species from Jujuy Province, NW Argentina. Mineralogical Magazine, 72, 1083–1101.
Palatinus, L. and Chapuis, G. (2007) Superflip. Applied Crystallography, 40, 786–790.
Pen'kov, I.N. and Safin, I.A. (1971) Study of franckeite ($Sn_3Pb_5Sb_2S_{14}$) by means of nuclear quadrupole resonance. Geokimiya, 1, 118–120 (in Russian).
Petříček, V. and Coppens, P. (1985) Structure analysis of displacively modulated molecular crystals. Acta Crystallographica, A41, 478–483.
——— (1988) Structure analysis of modulated molecular crystals. V. Symmetry restrictions for one-dimensionally modulated crystals. Acta Crystallographica, A44, 1051–1055.
Petříček, V., Malý, K., Coppens, P., Bu, X., Císařová, I, and Frost-Jensen, A. (1991) The description and analysis of composite crystals. Acta Crystallographica, A47, 210–216.
Petříček, V., Dušek, M., and Palatinus, L. (2006) Jana2006. Institute of Physics, Praha, Czech Republic.
Prior, G.T. (1904) On teallite, a new sulphostannite of lead from Bolivia and its relation to franckeite and cylindrite. Mineralogical Magazine, 14, 21–27.
Sachdev, S.C. and Chang, L.L.Y. (1975) Phase relations in the system tin-antimony-lead sulfides and the synthesis of cylindrite and franckeite. Economic Geology, 70, 1111–1122.
Shannon, R.D. (1981) Bond distances in sulfides and a preliminary table of sulfide crystal radii. In M. O'Keeffe and A. Navrotsky, Eds., Structure and Bonding in Crystals, 2, p. 53–40. Academic Press, New York.
Shimizu, M., Moh, G.H., and Kato, A. (1992) Potosiite and incaite from the Hoei Mine, Japan. Mineralogy and Petrology, 46, 155–161.
Smith, D.L. and Zuckermann, J.J. (1967) ^{119}Sn Mössbauer spectra of tin-containing minerals. Journal of Inorganic and Nuclear Chemistry, 29, 1203–1210.
Stelzner, A.W. (1893) Über Franckeit, ein neues Erz aus Bolivia. Neues Jahrbuch für Mineralogie, 2, 114–124.
Strunz, H. (1977) Mineralogische Tabellen. 6. Auflage, 621 p. Akademie Verlag, Leipzig.
van Smaalen, S. (1995) Incommensurate crystal structures. Crystallography Reviews, 4, 79–202.
Wang, S. (1989) Transmission electron microscope study of the minerals of the franckeite family. Ph.D. thesis, Chinese Geological University, Beijing (in Chinese).
Wang, S. and Kuo, K.H. (1991) Crystal lattices and crystal chemistry of cylindrite group minerals. Acta Crystallographica, A47, 281–392.
Wiedemeier, H. and von Schnering, H.G. (1978) Refinement of the structures of GeS, GeSe, SnS, and SnSe. Zeitschrift für Kristallographie, 148, 295–303.
Wiegers, G.A. and Meerschaut, A. (1992) Misfit layer compounds $(MS)_nTS_2$ (M=Sn, Pb, Bi, rare earth metals; T=Nb, Ta, Ti, V, Cr; 1.08<n<1.23): structures and physical properties. Materials Science Forum, 100/101, 101–172.
Williams, T.B. (1989) An electron microscope study of non-commensurate, double-layer, heavy-metal sulphides, 348 p. Ph.D. thesis. Australian National University, Canberra, A.C.T.
Williams, T.B. and Hyde, B.G. (1988) Electron microscopy of cylindrite and franckeite. Physics and Chemistry of Minerals, 15, 521–544.
Wolf, M., Hunger, H.J., Bewilogua, K. (1981) Potosiit-ein neues Mineral der Kylindrit–Franckeit–Gruppe. Freiberger Forschungshefte C, 364, 113–133.
Wu, G. and Huang, M. (1986) ^{119}Sn and ^{57}Fe Mössbauer studies of the franckeite from Dachang. Acta Petrologica et Mineralogica, 5, 345–352 (in Chinese).

Manuscript received February 25, 2011
Manuscript accepted August 10, 2011
Manuscript handled by Fernando Colombo